bioRxiv preprint doi: https://doi.org/10.1101/350801; this version posted October 1, 2018. The copyright holder for this preprint (which was not certified by peer review) is the author/funder, who has granted bioRxiv a license to display the preprint in perpetuity. It is made available under aCC-BY-NC-ND 4.0 International license.

Coherent chaos in a recurrent neural network with structured connectivity

Itamar Daniel Landau[1] and Haim Sompolinsky[1,2]

[1]Edmond and Lily Safra Center for Brain Sciences, The Hebrew University of Jerusalem, Jerusalem, Israel

[2]Center for Brain Science, Harvard University, Cambridge, MA, USA

bioRxiv preprint doi: https://doi.org/10.1101/350801; this version posted October 1, 2018. The copyright holder for this preprint (which was not certified by peer review) is the author/funder, who has granted bioRxiv a license to display the preprint in perpetuity. It is made available under aCC-BY-NC-ND 4.0 International license.

Abstract

We present a simple model for coherent, spatially correlated chaos in a recurrent neural network. Networks of randomly connected neurons exhibit chaotic fluctuations and have been studied as a model for capturing the temporal variability of cortical activity. The dynamics generated by such networks, however, are spatially uncorrelated and do not generate coherent fluctuations, which are commonly observed across spatial scales of the neocortex. In our model we introduce a structured component of connectivity, in addition to random connections, which effectively embeds a feedforward structure via unidirectional coupling between a pair of orthogonal modes. Local fluctuations driven by the random connectivity are summed by an output mode and drive coherent activity along an input mode. The orthogonality between input and output mode preserves chaotic fluctuations even as coherence develops. In the regime of weak structured connectivity we apply a perturbative approach to solve the dynamic mean-field equations, showing that in this regime coherent fluctuations are driven passively by the chaos of local residual fluctuations. Strikingly, the chaotic dynamics are not subdued even by very strong structured connectivity if we add a row balance constraint on the random connectivity. In this regime the system displays longer time-scales and switching-like activity reminiscent of "Up-Down" states observed in cortical circuits. The level of coherence grows with increasing strength of structured connectivity until the dynamics are almost entirely constrained to a single spatial mode. We describe how in this regime the model achieves intermittent self-tuned criticality in which the coherent component of the dynamics self-adjusts to yield periods of slow chaos. Furthermore, we show how the dynamics depend qualitatively on the particular realization of the connectivity matrix: a complex leading eigenvalue can yield coherent oscillatory chaos while a real leading eigenvalue can yield chaos with broken symmetry. We examine the effects of network-size scaling and show that these results are not finite-size effects. Finally, we show that in the regime of weak structured connectivity, coherent chaos emerges also for a generalized structured connectivity with multiple input-output modes.

Author Summary

Neural activity observed in the neocortex is temporally variable, displaying irregular temporal fluctuations at every accessible level of measurement. Furthermore, these temporal fluctuations are often found to be spatially correlated whether at the scale of local measurements such as membrane potentials and spikes, or global measurements such as EEG and fMRI. A thriving field of study has developed models of recurrent networks which intrinsically generate irregular temporal variability, the paradigmatic example being networks of randomly connected rate neurons which exhibit chaotic dynamics. These models have been examined analytically and numerically in great detail, yet until now the intrinsic variability generated by these networks have been spatially uncorrelated, yielding no large-scale coherent fluctuations. Here we present a simple model of a recurrent network of firing-rate neurons that intrinsically generates spatially correlated activity yielding coherent fluctuations across the entire network. The model incorporates random connections and adds a structured component of connectivity that sums network activity over a spatial "output" mode and projects it back to the network along an orthogonal "input" mode. We show that

bioRxiv preprint doi: https://doi.org/10.1101/350801; this version posted October 1, 2018. The copyright holder for this preprint (which was not certified by peer review) is the author/funder, who has granted bioRxiv a license to display the preprint in perpetuity. It is made available under aCC-BY-NC-ND 4.0 International license.

this form of structured connectivity is a general mechanism for producing coherent chaos.

Introduction

Firing-rate fluctuations and irregular spiking are ubiquitous in the neocortex[28, 3]. Furthermore this temporal variability is often observed to be correlated across spatial scales ranging from local cortical circuits to the entire brain: in local cortical circuits both in membrane potential fluctuations [40] and on the level of spiking [27, 4, 20, 21], in the coherency measured in brain-wide EEG signals [19, 1], and in the global signal observed across all voxels in fMRI measurements [26, 14, 18].

A class of theoretical models has successfully accounted for temporal variability via internally generated chaotic dynamics of recurrent networks, whether through excitation-inhibition balance in spiking models[38, 23] or the more abstract models of rate chaos in randomly connected networks[30]. Yet a key emergent feature of these models is the decorrelation of neural activity such that the macroscopic, population activity remains nearly constant in time. Population-wide coherence or synchrony can be generated in a variety of ways for example by introducing spatial modes with self-excitation, but this comes at a cost of drowning out the chaotic fluctuations and yielding fixed points [35]. Indeed a major challenge to theorists has been to produce network models which generate spatially coherent, temporally irregular fluctuations which can account for broad spatial correlations observed in experiments.

Two recent studies have shown that excitation-inhibition balance networks can generate spatially modulated correlations [25, 6]. In both of these studies the correlations are driven by common input from an external source, and the average correlation across the network remains small. It remains an open question whether a network can internally generate correlated fluctuations that are coherent across the entire network.

The chaotic dynamics of a network of randomly connected firing-rate neurons has been well-studied [30, 12]. In such a network each individual neuron's firing rate is given by a non-linear function of its input, which is in turn a weighted sum of the firing rates of all other neurons in the network. The network exhibits a phase transition from a fixed point to chaotic activity in which the randomness of the weights reverberates uncorrelated fluctuations throughout the network. Typically in this chaotic regime pairwise correlations are small and no coherent fluctuations emerge. Here we extend this model by adding a low-rank structured component of connectivity to the random connections. The structured connectivity sums the fluctuations along one spatial mode and projects them along a second, orthogonal mode yielding coherent fluctuations without drowning out the individual neuron variability which continues to drive the chaotic dynamics. A previous work studied a specific example of this structure and focused primarily on analyzing the non-chaotic regime[8]. Here we focus on the chaotic regime and show that

bioRxiv preprint doi: https://doi.org/10.1101/350801; this version posted October 1, 2018. The copyright holder for this preprint (which was not certified by peer review) is the author/funder, who has granted bioRxiv a license to display the preprint in perpetuity. It is made available under aCC-BY-NC-ND 4.0 International license.

this form of structured connectivity together with random connections provides a basic mechanism for internally generating coherent fluctuations.

Results

We study a network of N neurons in which the connectivity between neurons has two components: a random component, $\mathbf{J}$, and a rank-1 structured component, $\mathbf{M} = \frac{J_1}{\sqrt{N}}\boldsymbol{\xi}\boldsymbol{\nu}^T$, an outer product of a pair of orthogonal vectors both of which have elements of $O(1)$ and norm $\sqrt{N}$, with strength parameter J_1. We restrict the elements of $\boldsymbol{\xi}$ to be binary, $\xi_i = \pm 1$, which will be important for some of the results to come, and we will comment on when this restriction can be relaxed. We can think of the row vector, $\boldsymbol{\nu}^T$, as an "output mode" performing a read-out of the network activity, and the column vector, $\boldsymbol{\xi}$, as a corresponding "input mode" along which the output mode activity is fed back to the network (Fig 1A).

bioRxiv preprint doi: https://doi.org/10.1101/350801; this version posted October 1, 2018. The copyright holder for this preprint (which was not certified by peer review) is the author/funder, who has granted bioRxiv a license to display the preprint in perpetuity. It is made available under aCC-BY-NC-ND 4.0 International license.

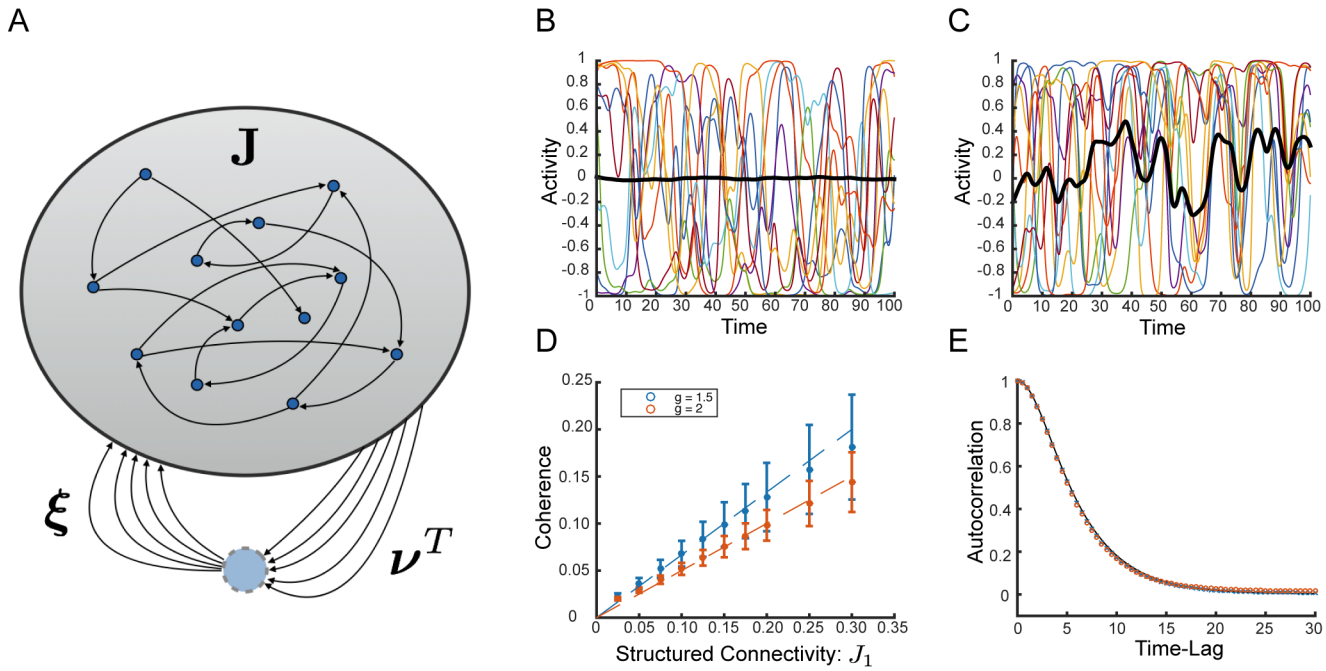

Figure 1. Random Network with Structured Connectivity Generates Coherent Chaos. (A) Network schematic showing neurons connected via random matrix $\mathbf{J}$ and rank-one structured connectivity. The structured component is represented schematically as a feed-forward loop with drive through the output mode, $\boldsymbol{\nu}$, and feedback through the input mode, $\boldsymbol{\xi}$. In our model these two vectors are orthogonal. The standard deviation of the random component is given by $\frac{g}{\sqrt{N}}$ and the strength of the structured component is $\frac{J_1}{\sqrt{N}}$. **(B)** Sample network dynamics without structured component, i.e. $J_1 = 0$, colored traces show a random collection of ten neural activity patterns, ϕ_j, black trace shows the coherent mode activity, $\bar{\phi} = \frac{1}{N}\boldsymbol{\xi}^T\boldsymbol{\phi}$. **(C)** Sample dynamics for $J_1 = 1$. Coherent mode displays substantial fluctuations. **(D)** Coherence, χ (definition in text), as a function of the strength of structured connectivity component, J_1 for small values of J_1. Simulation and theory (valid in the weak structured connectivity regime - $J_1 \ll g$) shown for both $g = 1.5$ and $g = 2$. Bars show standard deviation over 60 realization of the random connectivity. **(E)** Passive coherent chaos. With weak structured connectivity fluctuations of the coherent mode follow the fluctuations of the independent residual components. Normalized autocorrelation of the coherent component of the current, $\bar{q}(\tau)$, in red circles. Average normalized autocorrelation of the residuals, $q_\delta(\tau)$, in blue 'x's. Both are averaged over 60 realizations of the random connectivity with $J_1 = 0.1$. Prediction from theory in black. $N = 4000$ and $g = 2$ in all panels unless stated otherwise.

The random component of the connectivity is given by the matrix $\mathbf{J}$ consisting of identically distributed independent Gaussian elements with mean 0 and variance $\frac{g^2}{N}$, where g is an $O(1)$ parameter.

The state of each neuron is defined by its synaptic current, $h_i(t)$, with its firing rate given by $\phi_i \equiv \phi(h_i(t))$, where ϕ is a sigmoidal function. For some later results it will be necessary to assume that ϕ has a first derivative that is an even function. We therefore assume here for concreteness $\phi(h) = \tanh(h)$ unless otherwise noted, and we comment on when this assumption can be relaxed.

The dynamics of the synaptic current vector, $\mathbf{h}$, is given by

$$\frac{\mathrm{d}\mathbf{h}}{\mathrm{d}t} = -\mathbf{h} + \mathbf{J}\boldsymbol{\phi} + \frac{J_1}{\sqrt{N}}\boldsymbol{\xi}\boldsymbol{\nu}^T\boldsymbol{\phi} \tag{1}$$

bioRxiv preprint doi: https://doi.org/10.1101/350801; this version posted October 1, 2018. The copyright holder for this preprint (which was not certified by peer review) is the author/funder, who has granted bioRxiv a license to display the preprint in perpetuity. It is made available under aCC-BY-NC-ND 4.0 International license.

We have scaled the strength of the structured connectivity such that when the scaling-parameter $J_1 \sim O(1)$ the contribution of the structure to individual synapses is of the same order of magnitude as the typical random connection.

We will be particularly interested in the coherent activity and the coherent current, i.e. the spatial overlap of both the firing rate and the synaptic current with the input mode. These are defined respectively as

$$\bar{\phi} \equiv \frac{1}{N}\boldsymbol{\xi}^T\boldsymbol{\phi}, \quad \bar{h} \equiv \frac{1}{N}\boldsymbol{\xi}^T\mathbf{h}, \tag{2}$$

We define the measure of spatial coherence as the fraction of the total power of the network current h_i that is shared along the input mode, $\boldsymbol{\xi}$:

$$\chi \equiv \sqrt{\frac{\langle \bar{h}^2 \rangle}{\frac{1}{N}\sum_i \langle h_i^2 \rangle}} \tag{3}$$

where $\langle\ \rangle$ represents average over time. This is a useful measure as it varies from 0 to 1, and will yield $\chi = 1/\sqrt{N}$ for entirely independent, uncoupled fluctuations, and $\chi = 1$ for complete synchrony along $\boldsymbol{\xi}$.

Without the structured component, i.e. $J_1 = 0$, the network exhibits a phase transition at $g = 1$ from a zero fixed point to chaos[30]. In the chaotic state the randomness of the connectivity decorrelates the input current and yields an asynchronous state in which neurons fluctuate with negligible correlations such that both $\bar{\phi}$ and $\bar{h}$ are nearly constant in time, and $\chi \approx \frac{1}{\sqrt{N}}$ (Fig 1B).

Setting $J_1 = 1$, we observe significant correlations along the input mode, such that the coherent mode activity, $\bar{\phi}$, fluctuates significantly. For this network with $N = 4000$ we find the coherence $\chi \approx 0.4$, which is about 25 times larger than is observed in the asynchronous state. (Fig 1C).

In order to analyze this system we decompose the dynamics of the synaptic currents into coherent component, $\bar{h}$, and the vector of residuals currents, $\delta\mathbf{h} = \mathbf{h} - \bar{h}\boldsymbol{\xi}$. We also decompose the activity into its coherent component, $\bar{\phi}$, and vector of residual activity, $\delta\boldsymbol{\phi} = \boldsymbol{\phi} - \bar{\phi}\boldsymbol{\xi}$. Because of the orthogonality between input and output mode, the output mode ignores the coherent component, $\bar{\phi}$, and projects only the activity of the residuals: $\boldsymbol{\nu}^T\boldsymbol{\phi} = \boldsymbol{\nu}^T\delta\boldsymbol{\phi}$.

By averaging the dynamic equations 1 over the input mode, $\boldsymbol{\xi}$, we can write decomposed dynamics for the residual synaptic current vector and for the coherent current:

$$\frac{\mathrm{d}\delta\mathbf{h}}{\mathrm{d}t} = -\delta\mathbf{h} + \hat{\mathbf{J}}\boldsymbol{\phi} \tag{4}$$

$$\frac{\mathrm{d}\bar{h}}{\mathrm{d}t} \approx -\bar{h} + \frac{J_1}{\sqrt{N}}\boldsymbol{\nu}^T\delta\boldsymbol{\phi} \tag{5}$$

bioRxiv preprint doi: https://doi.org/10.1101/350801; this version posted October 1, 2018. The copyright holder for this preprint (which was not certified by peer review) is the author/funder, who has granted bioRxiv a license to display the preprint in perpetuity. It is made available under aCC-BY-NC-ND 4.0 International license.

where the effective connectivity matrix in the residual dynamics (discussed more fully in Methods) is

$$\hat{\mathbf{J}} \equiv \left(\mathbf{I} - \frac{\boldsymbol{\xi}\boldsymbol{\xi}^T}{N}\right)\mathbf{J} \tag{6}$$

which projects the output of $\mathbf{J}$ into the $(N-1)$ dimensional subspace orthogonal to $\boldsymbol{\xi}$. This guarantees that the decomposed dynamics satisfy the constraint $\boldsymbol{\xi}^T\delta\mathbf{h} = 0$. For most of what follows this constraint can be ignored as it contributes only $O\left(\frac{1}{\sqrt{N}}\right)$ to each synaptic current. Nevertheless it plays a role later and we introduce it here for completeness. We have, however, ignored the small projection of the random connectivity along the coherent mode ($\frac{\boldsymbol{\xi}^T}{N}\mathbf{J}\boldsymbol{\phi} \sim O\left(\frac{1}{\sqrt{N}}\right)$). Note that even in this approximation, the nonlinearity of ϕ in these equations couples the coherent and residual degrees of freedom.

In order to attempt to solve the approximate system we could assume that $\bar{h}(t)$ fluctuates according to some known random process and then consider the dynamics of the δh_i with the firing rate of individual units as given by $\phi\left(\delta h_i(t) + \xi_i\bar{h}(t)\right)$. However, for general J_1 we are unable to analytically close the loop and self-consistently compute the statistics of $\bar{h}(t)$.

Weak Structured Connectivity Yields Passive Coherent Chaos

In order to proceed analytically, we take a perturbative approach, assuming $J_1 \ll 1$. In this regime we assume the fluctuations in $\bar{h}(t)$ are Gaussian and we turn to computing the autocorrelations of both the coherent component

$$\bar{\Delta}(\tau) \equiv \left\langle \bar{h}(t)\,\bar{h}(t+\tau)\right\rangle \tag{7}$$

and of the residuals,

$$\Delta_\delta(\tau) \equiv \left\langle \delta h_i(t)\,\delta h_i(t+\tau)\right\rangle \ . \tag{8}$$

For small J_1 we assume that the coherent current is small ($\bar{h} \ll 1$) and therefore in the dynamics of the residual currents (Eqn 4) we approximate $\sum_j J_{ij}\phi_j \approx \sum_j J_{ij}\phi(\delta h_j)$. The result is that to leading order the autocorrelation of the residuals is given by the zeroth-order ($J_1 = 0$) autocorrelation. That is, the residual currents fluctuate as independent Gaussian processes almost identically to the situation without structured connectivity. These residual fluctuations are summed over the output mode yielding substantial fluctuations in $\boldsymbol{\nu}^T\delta\boldsymbol{\phi}$ (recall, $\nu_i \sim O(1)$). These in turn drive Gaussian fluctuations in the coherent mode and we show in Methods that its autocorrelation is given to first-order by

$$\bar{\Delta}(\tau) \approx \left(\frac{J_1}{g}\right)^2 \Delta_\delta(\tau) \tag{9}$$

bioRxiv preprint doi: https://doi.org/10.1101/350801; this version posted October 1, 2018. The copyright holder for this preprint (which was not certified by peer review) is the author/funder, who has granted bioRxiv a license to display the preprint in perpetuity. It is made available under aCC-BY-NC-ND 4.0 International license.

That is, to leading order the autocorrelation of the coherent component is simply a scaled version of the local, residual autocorrelation.

We verify this prediction numerically in Fig 1E for $J_1 = 0.1$ showing the normalized autocorrelations, $\bar{q}(\tau) = \frac{\bar{\Delta}(\tau)}{\bar{\Delta}(0)}$ and $q_\delta(\tau) = \frac{\Delta_\delta(\tau)}{\Delta_\delta(0)}$ as well as the prediction from theory. Qualitatively this means that in this regime chaos is driven by the emergent fluctuations in the local synaptic current similar to in the $J_1 = 0$ case, and that the coherent component can be said to absorb these fluctuations passively along the input mode, $\boldsymbol{\xi}$.

In this regime then, the coherence is given simply by

$$\chi = \sqrt{\frac{\bar{\Delta}(0)}{\bar{\Delta}(0) + \Delta_\delta(0)}} \approx \frac{J_1}{g} \tag{10}$$

Numerically, we find that this approximation provides a good description of the system's state for up to $J_1/g \approx 0.2$ (Fig 1D).

We can understand the coherent chaos in this regime qualitatively: the residual synaptic currents driven by the random connectivity fluctuate as uncorrelated Gaussian processes, and the resulting independent fluctuations in firing rates will be summed over the output mode, $\boldsymbol{\nu}$, which projects to the input mode, $\boldsymbol{\xi}$, driving coherent fluctuations in $\bar{h}(t)$. If the two modes, $\boldsymbol{\xi}$ and $\boldsymbol{\nu}$ had substantial overlap then the coherent fluctuations along $\boldsymbol{\xi}$ would drive positive feedback through $\boldsymbol{\nu}$ driving the neurons to a fixed point. The orthogonality of these modes effectively embeds a feedforward structure from the output mode, $\boldsymbol{\nu}$, to the input mode, $\boldsymbol{\xi}$, within the recurrent connectivity. This enables the persistence of stable fluctuations along the input mode, $\boldsymbol{\xi}$, which do not feedback to $\boldsymbol{\nu}$, thus preventing either saturation or oscillations.

Importantly, in the regime of passive coherence we can relax the restrictions on $\boldsymbol{\xi}$ and ϕ: Our results here hold for any smooth, sigmoidal non-linearity and for any $\boldsymbol{\xi}$ which is norm $\sqrt{N}$ and orthogonal to $\boldsymbol{\nu}$. In fact approximate orthogonality is sufficient in this regime: structured connectivity consisting of an outer product of two randomly chosen vectors will generate mildly coherent fluctuations.

Random Connectivity with "Row Balance"

We observe that as J_1 increases to values of $O(1)$, the network displays significant variability in the dynamics from realization to realization. The coherent mode autocorrelation function, $\bar{\Delta}(\tau)$, for example, is no longer self-averaging (Fig 2A). As we increase system size, N, we find that the realization-to-realization variability in $\bar{\Delta}(0)$

bioRxiv preprint doi: https://doi.org/10.1101/350801; this version posted October 1, 2018. The copyright holder for this preprint (which was not certified by peer review) is the author/funder, who has granted bioRxiv a license to display the preprint in perpetuity. It is made available under aCC-BY-NC-ND 4.0 International license.

saturates to a finite value (Fig 2B). Moreover, when $J_1 \gtrsim 1$ we observe realization-dependent transitions out of chaos to either fixed points or limit cycles (Fig 2C).

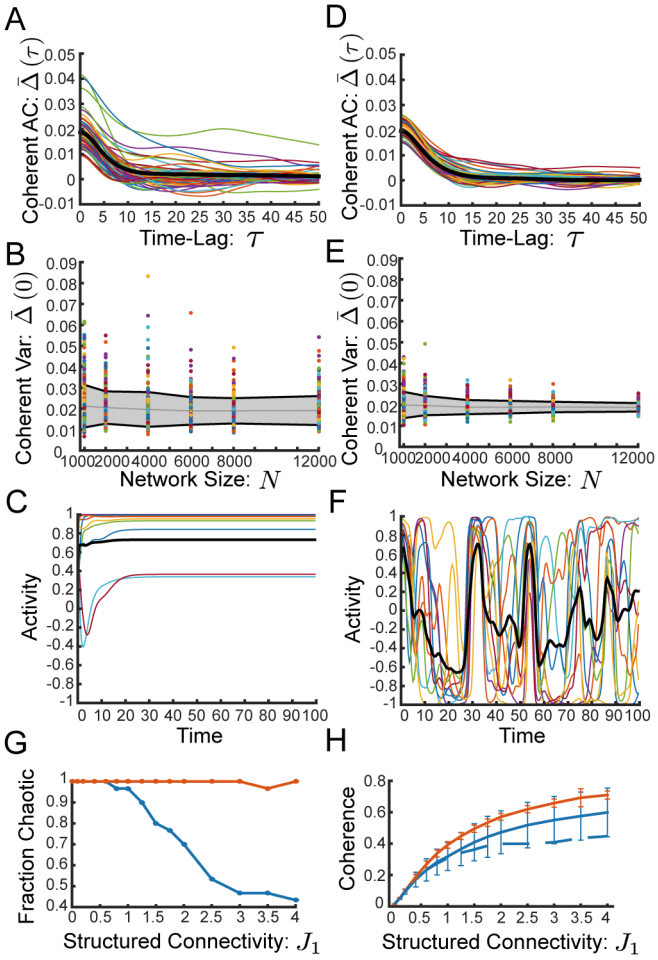

Figure 2. Row Balance Preserves Chaos, and Increases Coherence. (A) Full coherent mode autocorrelation, $\bar{\Delta}(\tau)$ of 60 individual realizations. Thick black line shows average over realizations. Network with random connectivity $\mathbf{J}$ without row balance exhibits significant difference between realizations **(B)** Coherent mode variance, $\bar{\Delta}(0)$, as a function of network size for 300 individual realizations. Gray line shows average and gray region with black boundary shows one standard deviation over realizations. Without row balance the standard deviation (over realizations) saturates to a finite value as the network size increases, indicating that the variability between realizations is not a finite-size effect. **(C)** Without row balance a network with moderate structured connectivity ($J_1 = 2.5$) exhibits a fixed point. **(D)-(F)** Same as (A)-(C) respectively, but network has "row balance" random connectivity, $\tilde{\mathbf{J}} = \mathbf{J} - \mathbf{J}\frac{\boldsymbol{\xi}\boldsymbol{\xi}^T}{N}$. **(D)** Individual realizations of $\Delta(\tau)$ are all very close to the average. **(E)** With row balance the standard deviation of $\Delta(0)$ over realizations shrinks with N, suggesting that the variability between realizations is a finite-size effect. **(F)** Same realization of $\mathbf{J}$ as in (C), but with row balance. Chaos is preserved. **(G)-(H)** Networks without row balance in blue, with row balance in red **(G)** Fraction of realizations (out of 30 realizations) that lead to chaotic dynamics, as a function of structural connectivity, J_1. Row balance keeps nearly all realizations chaotic. **(H)** Coherence, χ, as a function of J_1computed for the realizations from (E). Row balance increases coherence. Error bars display standard deviation. Full line shows all realizations, dashed line displays average coherence restricted to the chaotic realizations. $J_1 = 0.2$, $g = 2$, and $N = 4000$ for all panels unless otherwise noted.

The reason for this realization dependence is that as J_1 increases and the fluctuations in the coherent mode grow,

bioRxiv preprint doi: https://doi.org/10.1101/350801; this version posted October 1, 2018. The copyright holder for this preprint (which was not certified by peer review) is the author/funder, who has granted bioRxiv a license to display the preprint in perpetuity. It is made available under aCC-BY-NC-ND 4.0 International license.

feedback is generated through the interaction between the random connectivity, $\mathbf{J}$, and the input and output modes, $\boldsymbol{\xi}$ and $\boldsymbol{\nu}$. First of all, $\mathbf{J}$ maps the coherent activity back along the input mode with a small realization-dependent component which we ignored in Eqn 5 driving feedback directly to the coherent current, $\bar{h}$. Secondly, $\mathbf{J}$ maps the coherent activity along the the residuals in a realization-dependent direction biasing the residual fluctuations $\delta\mathbf{h}$. This direction in turn will have realization-dependent component along the output mode, $\boldsymbol{\nu}$, and therefore the coherent activity may additionally drive feedback by pushing the residual fluctuations along the output mode. See Methods for more details.

To suppress the strong realization dependence of the dynamics, we refine the random connectivity matrix by defining

$$\tilde{\mathbf{J}} \equiv \mathbf{J} - \mathbf{J}\frac{\boldsymbol{\xi}\boldsymbol{\xi}^T}{N} \tag{11}$$

This subtracts from each row of $\mathbf{J}$ its weighted average along the input mode. This "row balance" subtraction has been previously observed to remove realization-dependent outliers from the eigenspectrum of the full connectivity matrix [22, 34].

We find here that row balance suppresses realization-to-realization variability in the nonlinear chaotic dynamics, for example reducing the variability in the autocorrelation of the coherent mode, $\bar{\Delta}(\tau)$ (Fig 2D). We observe that with row balance this variability drops as a function of increasing system size, suggesting (although not proving) that the dynamics are now self-averaging in the limit of large N, at least for these values of J_1 (Fig 2E).

The impact of row balance on the chaotic dynamics can be understood by noting that the resulting connectivity matrix, $\tilde{\mathbf{J}}$, now has a null-space, and the input mode, $\boldsymbol{\xi}$, lies within it ($\tilde{\mathbf{J}}\boldsymbol{\xi} = 0$). The result of row balance then is to ensure that the random connectivity matrix filters out any coherent activity fluctuations, $\bar{\phi}(t)$:

$$\tilde{\mathbf{J}}\boldsymbol{\phi} = \left(\mathbf{J} - \mathbf{J}\frac{\boldsymbol{\xi}\boldsymbol{\xi}^T}{N}\right)\left(\bar{\phi}\boldsymbol{\xi} + \delta\boldsymbol{\phi}\right) = \mathbf{J}\delta\boldsymbol{\phi} \tag{12}$$

This prevents the coherent mode activity from driving feedback to the dynamics of the coherent current (Methods).

Interestingly, we find that row balance allows chaotic fluctuations to persist for larger values of J_1, whereas without row balance the majority of realizations exhibit fixed points or limit cycles for $J_1 \gtrsim 3$ (Fig 2F-G). Furthermore, the chaotic dynamics are more coherent with row balance than without (Fig 2H). As the structured connectivity is made stronger row balance appears to enable the dynamics to grow increasingly coherent even as chaotic fluctuations persist.

bioRxiv preprint doi: https://doi.org/10.1101/350801; this version posted October 1, 2018. The copyright holder for this preprint (which was not certified by peer review) is the author/funder, who has granted bioRxiv a license to display the preprint in perpetuity. It is made available under aCC-BY-NC-ND 4.0 International license.

Row Balance Yields Self-Tuned Coherent Chaos

When we increase the strength of structured connectivity, J_1, we find that with row balance the network yields chaotic dynamics which are strikingly coherent and display switching-like macroscopic activity (Fig 3A). In contrast to the case of weak structured connectivity, the coherent mode dynamics are no longer passively driven by the fluctuations in the residual synaptic currents. This is evidenced by the normalized autocorrelation of the coherent mode, $\bar{q}(\tau)$, which is no longer close to the normalized residual autocorrelation, $q_\delta(\tau)$, but rather has qualitatively different dynamics including longer time-scales (Fig 3B as compared to Fig 1E).

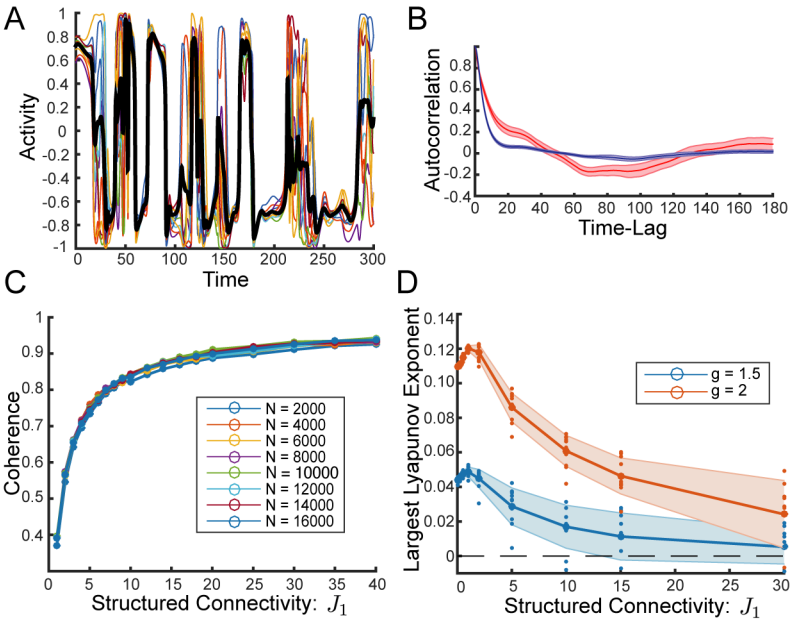

Figure 3. Strong Structured Connectivity with Row Balance Generates High Coherence Even as Chaos Persists. (A) Sample activity of 10 randomly chosen neurons, ϕ_j, and coherent mode activity, $\bar{\phi}$, in black. Strong structured connectivity with row balance subtraction to the random component of connectivity yields chaotic activity that is highly coherent with switching-like behavior. **(B)** Normalized autocorrelation of coherent mode, $\bar{q}(\tau)$, in red. Average normalized autocorrelation of the residuals, $q_\delta(\tau)$, in blue. Shaded regions show standard deviation over 25 initial conditions of the same connectivity. Strong structured connectivity yields coherent mode dynamics that are qualitatively different from those of the residuals. $J_1 = 15.8$ for both (A) and (B), compare to Fig 1C and Fig 1E, respectively. **(C)** Coherence, χ, as a function of J_1 is independent of network size. Coherence appears to approach 1 as J_1 is increased demonstrating that chaos persists even as fluctuations in the residuals shrink (See also Fig S4). Coherence is averaged over 30 realizations of the connectivity for each N, excluding the few fixed points and limit cycles that occur for larger J_1 (2 out of 30 or less for the largest values of N). **(D)** Largest Lyapunov exponent as a function of J_1. Thick line shows average over 10 realizations, small dots show values for individual realizations, and shaded region is standard deviation. All but a small fraction of realizations are chaotic, even in the region where $\chi > 0.9$. $N = 4000$ and $g = 2$ in all panels unless noted otherwise.

We find that the coherence, χ, increases steadily as a function of the strength of structured connectivity, J_1, and notably it is independent of system size. (Fig 3C).

bioRxiv preprint doi: https://doi.org/10.1101/350801; this version posted October 1, 2018. The copyright holder for this preprint (which was not certified by peer review) is the author/funder, who has granted bioRxiv a license to display the preprint in perpetuity. It is made available under aCC-BY-NC-ND 4.0 International license.

To check whether this highly coherent state is chaotic, we calculate the largest Lyapunov exponent and verify that the dynamics are indeed chaotic for a vast majority of realizations even as the fluctuations are highly coherent (Fig 3D).

We now examine the qualitative changes in the chaotic state of the network with row balance as J_1 increases. We observe that for $J_1 \lesssim 1$ the fluctuations are unimodal with an approximate Gaussian shape. The temporal fluctuations are dominated by a single time constant as with zero J_1 (Fig 4A-B). On the other hand, for larger values of J_1 the fluctuations deviate dramatically from Gaussian and instead become sharply bimodal (Fig 4A).

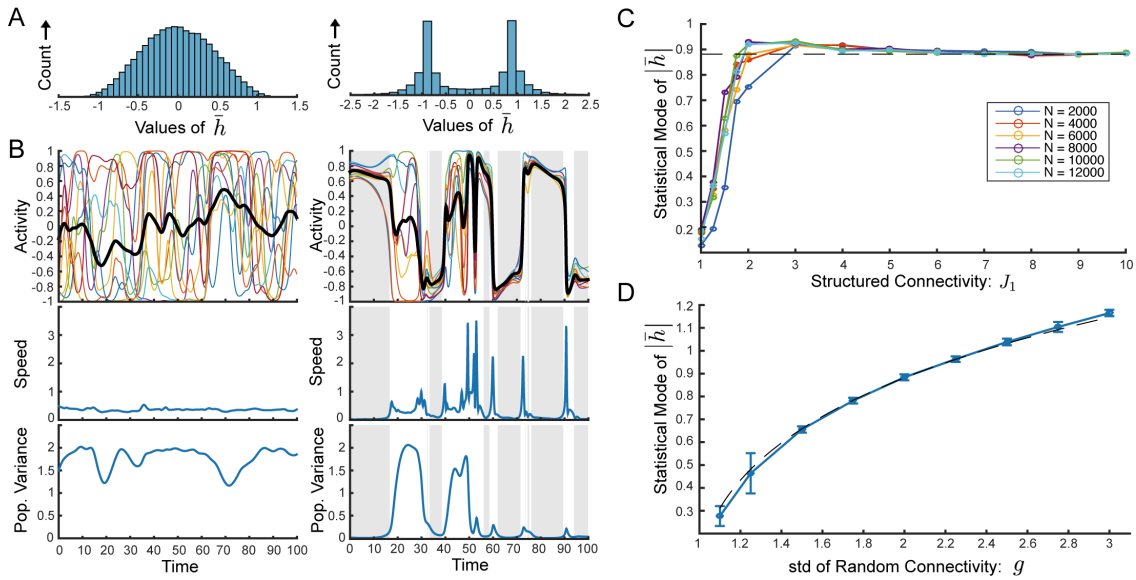

Figure 4. Self-Tuned Coherent Chaos. (A)-(B) Comparison between weak structured connectivity (Left: $J_1 = 0.8$) and stronger structured connectivity (Right: $J_1 = 15.8$). Both with $N = 4000$. **(A)** Histogram of values of the coherent mode current, $\bar{h}(t)$. Mild structured connectivity yields coherent fluctuations with a peak at zero and a distribution that appears not far from Gaussian. For stronger structured connectivity the histogram is clearly non-Gaussian and highly bimodal. **(B)** Top: Sample activity of 10 randomly chosen neurons, $\phi_i(t)$ and coherent mode activity, $\bar{\phi}(t)$. Middle: Speed of network during same epoch of activity, defined as the per-neuron norm of the rate-of-change vector, i.e. $\sqrt{\frac{1}{N}\sum_i \left(\frac{\mathrm{d}h_i}{\mathrm{d}t}\right)^2}$. Bottom: Instantaneous population variance of the residual currents $\delta h_i(t)$. For mild structured connectivity, $\bar{\phi}(t)$ fluctuates around zero (top), speed is roughly constant throughout the trial (middle), residual currents maintain large variance throughout (bottom). On the other hand, for stronger structured connectivity, there is state-switching between bouts of high and low coherent-mode activity (top), these same bouts are associated with vanishing speed (middle), and with small residual currents (bottom). **(C)** Statistical mode (most frequent value) of $|\bar{h}|$ as a function of J_1. The results indicate a crossover to self-tuned coherent chaos, defined by the bimodal peaks of $|\bar{h}|$ reaching a constant value. The crossover occurs very rapidly and independently of N. Dashed line shows $\bar{h}^c = \phi'^{-1}\left(\frac{1}{g}\right)$ **(D)** The statistical mode of $|\bar{h}|$ as a function of g with fixed $J_1 = 10$ and $N = 8000$. Dashed line shows $\bar{h}^c = \phi'^{-1}\left(\frac{1}{g}\right)$. $g = 2$ in all other panels.

Furthermore, we find that with larger values of J_1 the network exhibits intermittent switching between two different values of $\bar{h}$ (Fig 4B, top right). We observe that the dynamics at both of these values of $\bar{h}$ are qualitatively distinct

bioRxiv preprint doi: https://doi.org/10.1101/350801; this version posted October 1, 2018. The copyright holder for this preprint (which was not certified by peer review) is the author/funder, who has granted bioRxiv a license to display the preprint in perpetuity. It is made available under aCC-BY-NC-ND 4.0 International license.

as reflected by the speed of the dynamics and the level of coherence. We define the speed of the dynamics as the norm of the vector of first time-derivatives per neuron: $\sqrt{\frac{1}{N}\sum_i \left(\frac{\mathrm{d}h_i}{\mathrm{d}t}\right)^2}$. Similar measures have been used to find fixed points and slow dynamics in highly non-linear dynamics [32]. We observe that the two distinct values of $\bar{h}$ are both associated with vanishing speed (Fig 4B, middle right). Additionally they are associated with very high levels of coherence, i.e. small residuals as quantified by the population variance, $\frac{1}{N}\sum_i \left(\delta h_i\left(t\right)\right)^2$ (Fig 4B, bottom right). Evidently, in the network with larger values of J_1 there are two distinct states with slow dynamics and high levels of coherence, and the network switches rapidly between these two. In contrast, with mild structured connectivity both the speed and the variance of the residuals remain roughly constant throughout the trial (Fig 4B, left).

To gain insight into the emergence of the switching dynamics, we examine the most frequent value of $\left|\bar{h}\left(t\right)\right|$ as a function of J_1 and we find that there is a rapid crossover from a state with unimodal fluctuations around zero, to a state with bimodal peaks and that the most frequent value of $\left|\bar{h}\left(t\right)\right|$ saturates quickly with J_1 and then remains constant (Fig. 4C). What is the nature of this regime? And what determines the two values of $\bar{h}$ that come to dominate the dynamics?

Because the bouts of slow dynamics are associated with small residuals, we assume $\delta h_i \ll 1$ and approximate $\boldsymbol{\phi}\left(t\right) \approx \bar{\phi}\left(t\right)\boldsymbol{\xi} + \phi'\left(\bar{h}\left(t\right)\right)\delta\mathbf{h}$. Note that we have made use of the fact that $\xi_i = \pm 1$ and that ϕ is an odd function. Because $\boldsymbol{\xi}$ is in the null-space of the row-balanced connectivity ($\tilde{\mathbf{J}}\boldsymbol{\phi} = \mathbf{J}\delta\boldsymbol{\phi}$, as discussed above) the residual dynamics (Eqn 4) become

$$\frac{\mathrm{d}\delta\mathbf{h}}{\mathrm{d}t} = -\delta\mathbf{h} + \phi'\left(\bar{h}\right)\hat{\mathbf{J}}\delta\mathbf{h} \tag{13}$$

We observe that in these linearized dynamics the coherent mode current, $\bar{h}\left(t\right)$, plays the role of a dynamic gain via the slope of the transfer function, ϕ'.

In the linearized dynamics we turn to the eigenvectors, $\mathbf{u}^{(k)}$, of $\hat{\mathbf{J}}$ and decompose the residual dynamics according to $\delta\mathbf{h} = \sum_k c_k\mathbf{u}^{(k)}$. Given an instantaneous value of $\bar{h}$, the independent dynamics of the eigenmodes are

$$\frac{\mathrm{d}c_k}{\mathrm{d}t} = \left(-1 + \phi'\left(\bar{h}\right)\lambda_k\right)c_k \tag{14}$$

where λ_k is the kth eigenvalue of $\hat{\mathbf{J}}$. (We show in Methods that $\hat{\mathbf{J}}$ has the same eigenvalues as $\tilde{\mathbf{J}}$)

The leading eigenvalue, λ_1, has real part approximately equal to g. If $\bar{h}$ is small then $\phi'\left(\bar{h}\right) \approx 1$ and there are many modes that diverge exponentially. If $\bar{h}$ is large (either positive or negative) then $\phi'\left(\bar{h}\right) \approx 0$ and then all the modes decay exponentially. However, there are two critical values of $\bar{h}$ which yield marginal and therefore slow dynamics

bioRxiv preprint doi: https://doi.org/10.1101/350801; this version posted October 1, 2018. The copyright holder for this preprint (which was not certified by peer review) is the author/funder, who has granted bioRxiv a license to display the preprint in perpetuity. It is made available under aCC-BY-NC-ND 4.0 International license.

for the leading mode, c_1. These are the values, $\bar{h}^c$, for which the slope of the transfer function is equal to $\frac{1}{g}$:

$$\bar{h}^c = \phi'^{-1}\left(\frac{1}{g}\right) \tag{15}$$

If $\bar{h}(t) \approx \bar{h}^c$ and the residuals are small then the time constant of fluctuations in the leading eigenmode, $\left(1 - \phi'\left(\bar{h}\right) g\right)^{-1}$, are very long.

Indeed we find that the most frequent value of $\left|\bar{h}(t)\right|$ as a function of g fits the curve $h^c(g)$ very well (Fig. 4D).

We conclude that the switching between two states each with slow dynamics and a high level of coherence observed in Fig 4B reflects a regime of self-tuned coherent chaos in which the coherent mode self-adjusts to a critical value so that the dynamics of the small residuals are near-marginal, giving rise to slow dynamics. The above linearized dynamics (Eqn 13) are not exact and therefore non-linear interactions eventually destabilize the system and precipitate a state-switch. Nevertheless, the linearized dynamics dominate the dynamics of the small residuals during the bouts of high coherence.

As observed in Fig 4C, when we increase J_1, the most frequent value of $\left|\bar{h}(t)\right|$ rapidly increases until it saturates at a value very near to $\phi'^{-1}\left(\frac{1}{g}\right)$. Moreover, we find that this crossover to the regime of self-tuned coherent chaos occurs at moderate values of J_1 (on the order of g), independently of network size.

Notice the crucial role of row balance in facilitating self-tuned coherent chaos: row balance filters out the direct contribution of the coherent mode activity to the dynamics of the residuals and enables the coherent mode to act as a dynamic gain. The coherent mode then self-adjusts to cancel the leading eigenvalue of $\hat{\mathbf{J}}$ and yield bouts of slow, highly coherent dynamics.

We note that we can loosen the constraint on the symmetry of the transfer function and allow any smooth sigmoidal transfer function if we restrict the input mode to be uniform, $\xi_i = 1$ for all i. We show an example of the self-tuned coherent chaotic state for a non-symmetric transfer function in Fig S1.

Symmetry breaking in the self-tuned chaotic regime and transition to fixed point

The example of Fig. 4A illustrates dynamics which reside in the positive and negative coherent states with equal frequency, maintaining the $h_i \to -h_i$ symmetry of the underlying dynamic equations. We observe that in may realizations this symmetry is violated at the single trial level for sufficiently strong J_1, as demonstrated in Fig. 5A

bioRxiv preprint doi: https://doi.org/10.1101/350801; this version posted October 1, 2018. The copyright holder for this preprint (which was not certified by peer review) is the author/funder, who has granted bioRxiv a license to display the preprint in perpetuity. It is made available under aCC-BY-NC-ND 4.0 International license.

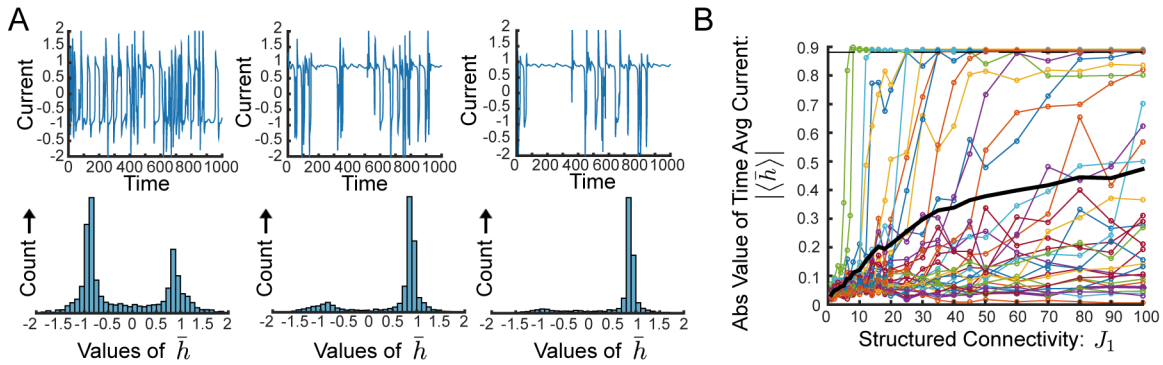

Figure 5. Realization-Dependent Symmetry Breaking in the Self-Tuned Chaotic Regime. (A) Sample traces of coherent mode current, $\bar{h}(t)$, (top) and histogram of values of $\bar{h}(t)$ (bottom) from a connectivity realization with real eigenvalue for $J_1 = 40, 60, 80$ increasing from left to right. Dynamics exhibit pronounced asymmetry. **(B)** Absolute value of the time-average coherent mode current, $\left|\langle \bar{h} \rangle\right|$, as a function of J_1. Each colored line represents a single connectivity realization, averaged over 10 initial conditions. For many individual realizations, $\left|\langle \bar{h} \rangle\right|$ is significantly non-zero over a large range of values of J_1, while still not arriving at fixed point value (displayed by dashed line). We display the 37 realizations with real leading eigenvalue out of 100 total realizations from this set of trials. Thick black line shows average over those realizations. $N = 8000$ for all panels.

We measure the asymmetry in a single trial as the absolute value of the *time-averaged* coherent activity, $\left|\langle \bar{h} \rangle\right|$, and we find that asymmetry grows gradually with J_1 throughout the chaotic regime, and at different rates for different realizations (Fig 5B).

As is evident in Fig. 5B, for many realization the level of asymmetry increases with J_1 until it reaches a maximal value of $\left|\langle \bar{h} \rangle\right| = \left|\bar{h}^c\right| = \left|\phi'^{-1}\left(\frac{1}{g}\right)\right|$(dashed line). At this point, the system spends all the time at one of the possible states, suggesting a transition to fixed point.

Indeed, as has been previously reported by Garcia Del Molino et al [8], realizations of $\hat{\mathbf{J}}$ that have a real leading eigenvalue (see also Methods) yield a fixed point equation for the above linearized dynamics (Eqns 13):

$$c_1^* \left(1 - \phi'\left(\bar{h}^*\right) \lambda_1\right) = 0 \tag{16}$$

The fixed point requires $\bar{h}^* = \bar{h}^c = \phi'^{-1}\left(\frac{1}{g}\right)$ so that all but the leading eigenmode decay to zero, and the resulting fixed point for c_1^* is marginally stable.

Indeed, we find that realizations of $\hat{\mathbf{J}}$ with a real leading eigenvalue undergo a transition to a fixed point upon sufficient increase of J_1. Similar to the preceding chaotic state, the fixed point is highly coherent, with very small residuals. Furthermore, it exhibits the hallmarks of the self-tuned coherent state: the value of the coherent mode is close to $\phi'\left(\bar{h}^*\right) = \frac{1}{g}$, the residuals are aligned with the leading eigenvector of $\hat{\mathbf{J}}$, and the the leading eigenvalue

bioRxiv preprint doi: https://doi.org/10.1101/350801; this version posted October 1, 2018. The copyright holder for this preprint (which was not certified by peer review) is the author/funder, who has granted bioRxiv a license to display the preprint in perpetuity. It is made available under aCC-BY-NC-ND 4.0 International license.

of the Jacobian matrix at the fixed point is close to zero (Fig S2).

Oscillatory fluctuations in self-tuned chaos and transition to limit cycle

The above symmetry breaking and transition to fixed point is observed only for some of the realizations of $\mathbf{J}$. In most of the other cases, rather than symmetry breaking, we observe an increased oscillatory component in the chaotic dynamics. This is reflected in the presence of a large second peak in the normalized autocorrelation function, $\bar{q}(\tau)$ (Fig 6A).

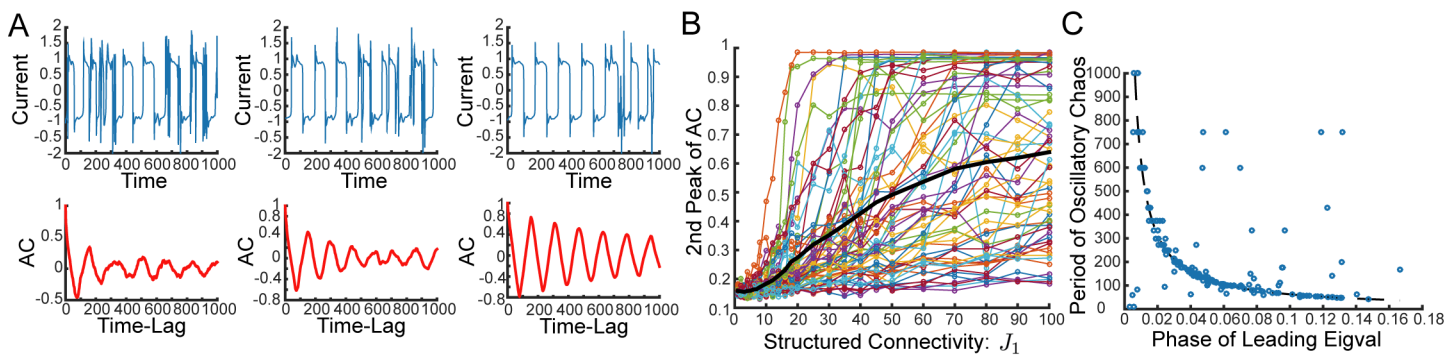

Figure 6. Realization-Dependent Oscillatory Imprint on the Self-Tuned Chaotic Regime. (A) Sample traces $\bar{h}(t)$ (top), and normalized autocorrelation $\bar{q}(\tau)$ (bottom) of coherent mode current for a connectivity realization with complex eigenvalue for $J_1 = 25, 30, 35$ increasing from left to right. Dynamics exhibit pronounced oscillatory power and the autocorrelation exhibits a pronounced peak near the same frequency that will dominate the limit cycle for larger J_1. **(B)** Height of second peak of the autocorrelation of the coherent mode input as a function of J_1. Each colored line represents a single connectivity realization, averaged over 10 initial conditions. For many realizations, there is a significant second peak in the autocorrelation over a long range of values of J_1 well before a limit cycle is reached. We display the 63 realizations which had complex leading eigenvalue out of 100 in this set of trials. Thick black line shows average over those realizations. **(C)** Observed period of oscillatory chaos vs phase of leading eigenvalue for 181 realizations from which we were able to measure an oscillatory period with chaotic fluctuations (out of 196 realizations with complex leading eigenvalue in this set of trials. In order to confine to realizations and values of J_1 that yielded chaos, we restrict to those with second peak of autocorrelation less than 0.8. These had average height of second peak over all realizations: 0.5). Dotted line shows prediction from theory: $\frac{2\pi}{\text{Phase}(\lambda_1)}$. The bulk of realizations are very well predicted although a notable fraction are not. The median error of prediction was 7.75 (average period over these realizations: 231, std: 212). $N = 8000$ for all panels.

The origin of these oscillations can be traced to the nature of the leading eigenvalues of $\hat{\mathbf{J}}$. As also reported in [8] and elaborated in Methods, if the leading eigenvalue of $\hat{\mathbf{J}}$, λ_1, is complex then there is no fixed point solution. Instead we assume in this case that $\bar{h}(t)$ undergoes a limit cycle with period T and find the solution for $c_1(t)$:

$$c_1(t) = c_1(0)\exp\left(-t + \Phi(t)\lambda_1\right) \tag{17}$$

where $\Phi(t) = \int_0^t ds\, \phi'\left(\bar{h}(s)\right)$.

bioRxiv preprint doi: https://doi.org/10.1101/350801; this version posted October 1, 2018. The copyright holder for this preprint (which was not certified by peer review) is the author/funder, who has granted bioRxiv a license to display the preprint in perpetuity. It is made available under aCC-BY-NC-ND 4.0 International license.

Requiring that this yield a limit cycle solution for $c_1(t)$ with period T yields

$$T = 2\pi \frac{\mathrm{Re}\lambda_1}{\mathrm{Im}\lambda_1} \tag{18}$$

and this additionally requires that the period-average of $\phi'\left(\bar{h}(t)\right)$ to be equal to the critical value $\frac{1}{g}$.

Indeed, we observe that in the case of a $\hat{\mathbf{J}}$ with complex leading eigenvalue, most realizations exhibit oscillatory fluctuations. The height of the second peak in the autocorrelation, $\bar{q}(\tau)$, grows gradually with J_1 with a realization-dependent rate (Fig 6B). Furthermore, for most individual realizations the period of the dominant oscillatory peak in the autocorrelation, even within the chaotic regime, is well-predicted by the above theoretical prediction for T (Eqn 18, Fig 6C).

For for indivdual realizations, there is a sufficiently large J_1 beyond which the second peak of $\bar{q}(\tau)$ reaches 1 and the dynamics transition to a pure limit cycle (Fig S3). We note that some realizations with a real leading eigenvalue also exhibit oscillatory components in their chaotic dynamics for certain values of J_1, which we presume relate to complex subleading eigenvalues, but these do not exhibit a transition to pure limit cycle (data not shown).

Realization-dependence and system-size scaling of the transition out of chaos

We now consider the critical value, J_1^c, of the strength of structured connectivity that yields a transition out of chaos. In contrast to the case without row balance, we find that in the row-balanced network the transition out of chaos occurs at values of J_1 scaling at least as $\sqrt{N}$. However, the particular value of J_1^c varies considerably across realizations (Fig S2 and S3).

The case of a real leading eigenvalue $\lambda_1 \approx g$ and the associated transition to fixed point provides a starting point for analyzing the transition out of chaos (a similar argument is made in the Methods for the case of complex leading eigenvalue). In the limit of small residual currents, $\delta h_i \ll 1$, the fixed point equation for the coherent mode current (5) is $\bar{h}^* = \phi'\left(\bar{h}^*\right) \frac{J_1}{\sqrt{N}} \boldsymbol{\nu}^T \delta\mathbf{h}^*$. Applying the fixed point requirements derived above that $\phi'\left(\bar{h}^*\right) = \frac{1}{g}$ and $\delta\mathbf{h} = c_1^* \mathbf{u}^{(1)}$, where $\mathbf{u}^{(1)}$ is the leading eigenvector of $\hat{\mathbf{J}}$, we find (as also reported in [8]) that

$$c_1^* = \frac{\sqrt{N} g \phi'^{-1}\left(\frac{1}{g}\right)}{J_1 \boldsymbol{\nu}^T \mathbf{u}^{(1)}} \tag{19}$$

bioRxiv preprint doi: https://doi.org/10.1101/350801; this version posted October 1, 2018. The copyright holder for this preprint (which was not certified by peer review) is the author/funder, who has granted bioRxiv a license to display the preprint in perpetuity. It is made available under aCC-BY-NC-ND 4.0 International license.

Equation 19 suggests that J_1^c scales as inverse of the overlap between the leading eigenvector, $\mathbf{u}^{(1)}$, and the output mode, $\boldsymbol{\nu}$. Indeed, we show numerically that the critical value J_1^c for fixed g is negatively correlated with $\left|\boldsymbol{\nu}^T\mathbf{u}^{(1)}\right|$ (Fig 7A).

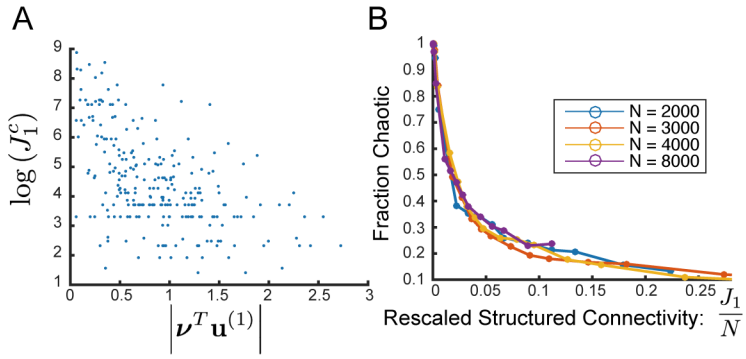

Figure 7. Sufficiently Strong Structure Yields Transition Out of Chaos Despite Row Balance: (A) Scatterplot of the logarithm of transitional value of J_1 vs the absolute value of the projection of the output mode, $\boldsymbol{\nu}$, on the leading eigenvector, $\mathbf{u}^{(1)}$ for 300 connectivity realizations with $N = 8000$. $r^2 = 0.29$. **(B)** Fraction of realizations displaying chaotic activity as a function of the rescaled structured connectivity: $\frac{J_1}{N}$. With this scaling the curve appears to be independent of N.

We next ask how J_1^c scales with system size. Because the above fixed point assumes $\delta h_i = c_1 u_i^{(1)} \ll 1$ where $\mathbf{u}^{(1)}$ has norm 1, we must have c_1 be no larger than $O(1)$. Since the typical value of $\left|\boldsymbol{\nu}^T\mathbf{u}^{(1)}\right|$ is $O(1)$ we would naively expect that the typical transition might occur for $J_1^c \sim \sqrt{N}$. However, we observe numerically that the fraction of realizations exhibiting chaotic dynamics for a given value of J_1 appears to scale as $\frac{J_1}{N}$ and not as $\frac{J_1}{\sqrt{N}}$ as expected (Fig 7B). For finite N chaos appears to be lost for some $J_1^c \sim N^\alpha$ with $\alpha \in [1/2, 1]$, and the particular J_1^c is highly realization-dependent. An analytical derivation of the actual value of J_1^c requires a more comprehensive study of the network's stability.

From our numerical work it appears that in the limit of large system size chaos persists for all values of J_1, for almost all realizations. Indeed for a network with $N = 16000$, for example, we increase J_1 up to values around 100 and observe that chaos persists for most realizations and coexists with a very high degree of spatial coherence. The coherence measure, χ, reaches values higher than 0.96 even as fluctuations persist (Fig S4). Thus we conjecture that in the limit $N \to \infty$, for almost all realizations, increasing J_1 indefinitely will yield self-tuned coherent chaos with $\chi \to 1$.

bioRxiv preprint doi: https://doi.org/10.1101/350801; this version posted October 1, 2018. The copyright holder for this preprint (which was not certified by peer review) is the author/funder, who has granted bioRxiv a license to display the preprint in perpetuity. It is made available under aCC-BY-NC-ND 4.0 International license.

Multiple Modes of Coherence

We generalize our model in order to construct a network with multiple modes of coherent activity. In this extension we take the structural component, $\mathbf{M}$, to be a low-rank matrix comprised of the sum of outer products of pairs of vectors which are all mutually orthogonal:

$$\mathbf{M} = J_0 \sum_{k=1}^{d} \frac{w_k}{\sqrt{N}} \boldsymbol{\xi}^{(k)} \boldsymbol{\nu}^{(k)^T} \tag{20}$$

where we have introduced a parameter J_0 that controls the overall strength of the structured connectivity, and a set of parameters w_k satisfying $\sum_{k=1}^{d} w_k^2 = 1$ that determine the relative weight of the different modes.

We can extend our schematic representation and think of each row vector $\boldsymbol{\nu}^{(k)^T}$ as a separate output mode connected in a feed-forward-like manner to the input mode, $\boldsymbol{\xi}^{(k)}$, (Fig 8A) and then decompose the dynamics into the residual dynamics identical to the above (Eqn 4) and the dynamics of the coherent activity along each separate input mode:

$$\frac{\mathrm{d}\bar{h}^{(k)}}{\mathrm{d}t} = -\bar{h}^{(k)} + \frac{J_0 w_k}{\sqrt{N}} \boldsymbol{\nu}^{(k)^T} \boldsymbol{\phi} \tag{21}$$

where each separate coherent current is given by $\bar{h}^{(k)} \equiv \frac{1}{N} \boldsymbol{\xi}^{(k)^T} \mathbf{h}$.

bioRxiv preprint doi: https://doi.org/10.1101/350801; this version posted October 1, 2018. The copyright holder for this preprint (which was not certified by peer review) is the author/funder, who has granted bioRxiv a license to display the preprint in perpetuity. It is made available under aCC-BY-NC-ND 4.0 International license.

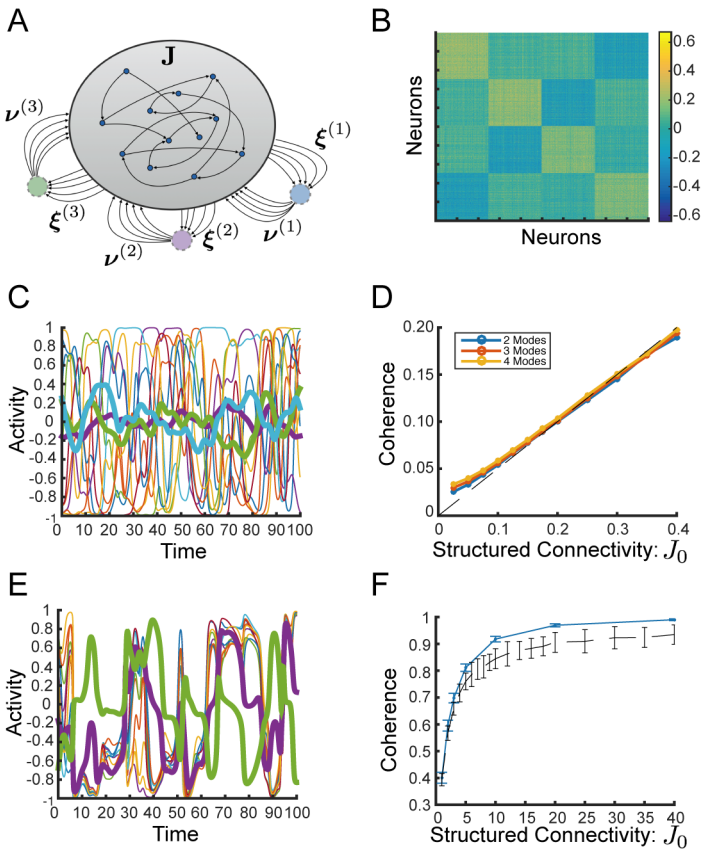

Figure 8. Coherent Chaos Along Multiple Modes. **(A)** Schematic of network with three coherent modes displaying effective output modes, $\boldsymbol{\nu}^{(k)}$, and input modes, $\boldsymbol{\xi}^{(k)}$, each of which are orthogonal to all others. **(B)** Matrix of Pearson correlation coefficients between firing rates, ϕ_i, of pairs of neurons in a network with three coherent modes and $J_1 = 1$. **(C)** Sample activity trace displaying sample single neuron activities and in thicker lines, three coherent mode activities, $\bar{\phi}^{(k)}$. **(D)** Generalized coherence, $\chi^{(k)}$, as a function of J_1 for 2, 3, 4 modes in the regime of passive coherence. Dashed line displays theory. **(E)** Sample activity traces display extreme coherence for two coherent modes. **(F)** Generalized coherence for two coherent modes (in blue) as a function of J_1 extends to near complete coherence, while chaos persists. Compare network with one coherent mode (in black dashed line). Bar shows standard deviation over 100 realizations. For panels **(B)**, **(C)**, **(E)** $N = 2000$. For panels **(D)** and **(F)** $N = 4096$.

The analytical results found above for the regime of passive coherence can be directly extended to the case of multiple modes. In particular, in the limit where $J_0 \ll 1$, the separate coherent modes are independent of each other and driven passively by the residual fluctuations (Fig 8C) such that

$$\bar{\Delta}^{(k)}(\tau) \approx \frac{J_0^2}{g^2} w_k^2 \Delta_\delta(\tau) \tag{22}$$

where $\bar{\Delta}^{(k)}(\tau) = \left\langle \bar{h}^{(k)}(t)\, \bar{h}^{(k)}(t+\tau) \right\rangle$ is the autocorrelation function of the kth coherent mode.

The resulting covariance matrix, $C_{ij} \equiv \langle \phi_i \phi_j \rangle$, has a low-rank structure which is shaped by the input modes (Fig

bioRxiv preprint doi: https://doi.org/10.1101/350801; this version posted October 1, 2018. The copyright holder for this preprint (which was not certified by peer review) is the author/funder, who has granted bioRxiv a license to display the preprint in perpetuity. It is made available under aCC-BY-NC-ND 4.0 International license.

8B). In particular, by Taylor expanding ϕ_i around δh_i:

$$C_{ij} \approx \left\langle \left(\phi\left(\delta h_i\right) + \phi'\left(\delta h_i\right) \sum_k \bar{h}^{(k)} \xi_i^{(k)} \right) \left(\phi\left(\delta h_j\right) + \phi'\left(\delta h_j\right) \sum_k \bar{h}^{(k)} \xi_j^{(k)} \right) \right\rangle \tag{23}$$

Since the residuals are on average uncorrelated and the distinct input modes are orthogonal, we find using Eqn 22 that to leading order:

$$\mathbf{C} \approx \left[\phi'\right]_{\mathbf{J}}^2 \Delta_\delta\left(0\right) \frac{J_0^2}{g^2} \sum_{k=1}^{d} w_k^2 \boldsymbol{\xi}^{(k)} \boldsymbol{\xi}^{(k)^T} \tag{24}$$

We generalize our measure of coherence to measure the d-dimensional coherence, or the fraction of total power which is shared along the d input mode directions:

$$\chi^{(d)} \equiv \sqrt{\frac{\sum_{k=1}^{d} \left\langle \left(\bar{h}^{(k)}\right)^2 \right\rangle}{\frac{1}{N}\sum_i \left\langle h_i^2 \right\rangle}} \tag{25}$$

and we find that for $J_k \ll g$ and finite d

$$\chi^{(d)} \approx \frac{J_0}{g} \tag{26}$$

Numerically, this prediction holds well for up to $\frac{J_0}{g} = 0.2$ for at least up to $d = 4$ as we show in Fig 8D, and we expect it to hold for larger d as well.

We note that in the regime of passive coherence, just as in the case of a single coherent mode, we can relax the restrictions on $\boldsymbol{\xi}^{(k)}$ and ϕ: Our results hold for $\boldsymbol{\xi}^{(k)}$ any norm $\sqrt{N}$ vector orthogonal to $\boldsymbol{\nu}^{(j)}$ $\forall j$ and $\boldsymbol{\xi}^{(j)}$ $j \neq k$, and also for ϕ any sigmoidal function.

In addition, we can generalize row balance by subtracting the weighted row-average for each input mode such that every $\boldsymbol{\xi}^{(k)}$ will reside in the null space of the new connectivity matrix, $\tilde{\mathbf{J}}^{(d)}$:

$$\tilde{\mathbf{J}}^{(d)} \equiv \mathbf{J} - \mathbf{J}\frac{1}{N}\sum_{k=1}^{d} \boldsymbol{\xi}^{(k)} \boldsymbol{\xi}^{(k)^T} \tag{27}$$

For $d > 2$ this generalized row balance does not appear to preserve chaotic fluctuations and instead fixed points or limit cycles appear for $J_0 \sim O\left(1\right)$.

Intriguingly, for $d = 2$ we observe that with generalized row balance the chaotic regime persists as the structured connectivity is strengthened and the dynamics become increasingly coherent. The dynamics display switching-like activity in which at any time one of the two coherent modes appears to be near the critical value h^c while the other mode is near zero (Fig 8E). It appears that the generalized coherence approaches 1 while chaos persists (Fig 8F)

bioRxiv preprint doi: https://doi.org/10.1101/350801; this version posted October 1, 2018. The copyright holder for this preprint (which was not certified by peer review) is the author/funder, who has granted bioRxiv a license to display the preprint in perpetuity. It is made available under aCC-BY-NC-ND 4.0 International license.

such that we conjecture that just as in the case of $d = 1$, here too in the large N limit $\chi^{(2)} \to 1$ as $J_0 \to \infty$.

Discussion

Coherent fluctuations are prevalent in cortical activity ranging in spatial scale from shared variability in membrane potential and spiking in local circuits to global signals measured across the scalp via EEG or across voxels via fMRI [40, 27, 1, 14]. Constructing a model that intrinsically generates coherent fluctuations has been a challenge to theorists.

We have studied the intrinsic generation of coherent chaotic dynamics in recurrent neural networks. Our model consists of rate-based neurons whose recurrent connections include a structured component in addition to random connections. The structured component is a low-rank connectivity matrix consisting of outer products between orthogonal pairs of vectors which allow local fluctuations to be summed along an output mode, amplified and projected to an input mode resulting in coherent fluctuations. The orthogonality of input and output mode effectively embeds a purely feedforward structure within the recurrent connectivity, thus avoiding feedback of the coherent fluctuations along the input mode.

In the regime where the structured component is weak, the local synaptic currents are effectively uncoupled from the coherent mode activity and their dynamics are similar to that of a random network with no structured component at all. The local fluctuations are summed by the structured component of connectivity to drive the coherent mode, which follows those fluctuations in a passive manner. In this regime of passive coherent chaos we derive a perturbative dynamical mean-field theory following [30, 12] which shows that the coherence grows linearly with the ratio of the strength of structured connectivity to the random connectivity. We show that this analysis extends to multiple modes of coherent activity yielding a finite-rank covariance pattern for the coherent fluctuations.

For moderate strength of structured connectivity the network exhibits significant realization-dependence and most realizations transition to either a fixed point or a limit cycle. A realization-dependent theory of these transitions is beyond the scope of this work. We add a row-balance constraint, placing the input mode in the null-space of the random connectivity matrix, and we observe that this constraint preserves chaos, reduces the variability between realizations, and increases the level of coherence.

With row balance, increased strength of structured connectivity yields a crossover to a distinct regime of self-tuned coherent chaos. In this regime the network undergoes Up-Down-like switching between two states each of

bioRxiv preprint doi: https://doi.org/10.1101/350801; this version posted October 1, 2018. The copyright holder for this preprint (which was not certified by peer review) is the author/funder, who has granted bioRxiv a license to display the preprint in perpetuity. It is made available under aCC-BY-NC-ND 4.0 International license.

which are characterized by slow, highly coherent dynamics. We show how row balance facilitates this regime by enabling the coherent mode to act as a dynamic gain to the dynamics of the residual currents. Consequently, intermittent marginal dynamics emerge as the coherent mode self-adjusts to one of two critical values. Interestingly the crossover to this self-tuned coherent regime happens for moderate strength of structured connectivity, independently of network size.

In the regime of self-tuned coherent chaos, realization-dependent qualitative differences begin to emerge with increasing strength of structured component, J_1. For realizations of the row-balanced random connectivity with real leading eigenvalue, symmetry-breaking emerges such that individual initial conditions yield trajectories that spend more time near one of the critical values of the coherent mode than the other. For realizations with complex leading eigenvalue, oscillatory fluctuations begin to emerge. The frequency of these oscillations is well predicted by the phase of the leading eigenvalue. Note that we have not addressed the question of the necessary scaling of J_1 for the emergence of realization-dependence in the chaotic regime for the limit of large system size.

As structured connectivity is further strengthened chaos persists even as coherence continues to increase until the dynamics are dominated almost entirely by the one dimensional fluctuations of the coherent mode. For a finite network, above some critical strength of the structured component the system converges to either a fixed point or a limit cycle, depending on the leading eigenvalue of the row-balanced random connectivity. Our numerical work suggests that the critical strength of structured connectivity grows with the system size, most likely scaling as $J_1^c \sim N$ (at least as $J_1^c \sim \sqrt{N}$). Hence we conjecture that for the scaling of the strength of structured connectivity presented here, as the network size diverges coherent chaos persists independent of J_1 for most realizations, and the level of coherence can be brought arbitrarily close to 1.

Importantly, in the regime of weak structured connectivity and passive coherence some of the assumptions of our model can be loosened. First, in this regime row balance on the random connectivity is not necessary. Additionally, we need not require the input mode be binary but rather any general pair of orthogonal vectors can serve as input and output mode. Moreover we can loosen the restriction on orthogonality: a random pair of vectors can be used without qualitative impact on the dynamics presented here because the contribution of the realization-dependent overlap between the two vectors in this regime will be negligible relative to the typical contribution from the full-rank random connectivity, $\mathbf{J}$.

On the other hand, achieving self-tuned and highly coherent chaos requires the network be finely-tuned to a high degree. The orthogonality of the input and output modes is not enough in order to achieve highly coherent chaos because of interactions between the random and structured components of connectivity. We therefore constrain the

bioRxiv preprint doi: https://doi.org/10.1101/350801; this version posted October 1, 2018. The copyright holder for this preprint (which was not certified by peer review) is the author/funder, who has granted bioRxiv a license to display the preprint in perpetuity. It is made available under aCC-BY-NC-ND 4.0 International license.

random component to satisfy row balance by ensuring that the input mode of the structured connectivity be in the null-space of the random component of connectivity. In addition to row balance, the self-tuned coherence regime depends on the choice of the single-neuron transfer function and input-mode vector. In the case where the transfer function is an odd function, such as tanh used throughout the main text, the input mode can be any binary vector. Otherwise, high coherence is achieved only for a uniform input mode, $\xi_i = 1\,\forall i$. In the latter case, the theory developed here predicts coherent fluctuations that switch between two non-symmetric values of the coherent mode, corresponding to the two points where where the slope of the transfer function equals $1/g$, and we have verified this numerically (Fig S1).

An interesting question is whether the particular structure of the connectivity matrix in our model can be achieved by a biologically plausible synaptic learning rule. Prior studies of sequence generation have constructed learning rules that yield connectivity which is comprised of outer-products of random vectors [29, 33] and these could form the basis for learning the necessary orthogonal rank-one structure. Plausible learning rules for yielding balanced excitation-inhibition dynamics [39, 15, 13] could potentially provide a foundation for learning row balance. It is thus plausible that the constraints of our model can be achieved by an appropriate synaptic learning, especially for the more robust regime of mild coherence. On the other hand, it is unclear to us whether the high degree of fine tuning required for the self-tuned coherence regime can be achieved by a biologically plausible learning rule. Investigating candidates of appropriate learning rules for generating coherent chaos, is beyond the scope of this work.

In the case of a uniform input mode the model can be constructed as an excitation-inhibition network, for example with half the neurons defined as excitatory by setting $\nu_i = 1$ and the other half defined as inhibitory via $\nu_i = -1$ (or a larger inhibitory value to compensate for a smaller fraction of inhibitory neurons). From this perspective the coherent fluctuations, in particular in the regime of passive coherence, can be understood within the framework of dynamic excitation-inhibition balance [38]. In this case the pair of balance equations are degenerate and constrain only the mean excitatory population rate to be nearly equal the inhibitory rate, but otherwise leave the overall mean rate unconstrained. Local residual fluctuations yield only small differences in mean population rates, thus leaving the balance satisfied, but these small differences drive significant coherent fluctuations because of the strong balanced connectivity. In the general setting of excitation-inhibition balance the pair of balance equations fully determine the mean rates to leading order and no coherent fluctuations are possible without introducing shared fluctuations in the external drive. We note that excitation-inhibition networks in the literature have sometimes been constructed yielding degenerate balance equations. As we have shown here, such choices have dramatic impact on the dynamics and the results should not be assumed to be generalizable.

In parallel to our study a pre-print has been published which explores a very similar model[10]. The authors observe

bioRxiv preprint doi: https://doi.org/10.1101/350801; this version posted October 1, 2018. The copyright holder for this preprint (which was not certified by peer review) is the author/funder, who has granted bioRxiv a license to display the preprint in perpetuity. It is made available under aCC-BY-NC-ND 4.0 International license.

a similar phenomenon as the self-tuned coherence studied here, and attempt to explain it by an iterative numerical solution of locally Gaussian dynamic mean-field equations. They do not make the role of row balance clear in their analysis. In contrast, we have focused on analytical solutions in the limit of both weak and strong structured connectivity, deriving a perturbative dynamic mean-field solution for the regime of weak structure and passive coherence. As we have shown here row balance is critical for moderate structure and self-tuned coherent chaos. Additionally we have shown that a full understanding of the properties of the highly coherent regime requires a realization-dependent mean-field analysis. In particular, we have explained that the leading eigenvalue of the row-balanced random connectivity matrix impacts qualitative features of the chaotic dynamics, yielding either broken symmetry or oscillatory fluctuations. Furthermore the critical strength of structured connectivity that leads to a transition to either fixed point or limit cycle is correlated with the extent of overlap between the leading eigenvector and the output mode.

As mentioned in the main text and introduction, a previous study also explored the case of a single orthogonal E-I structured component[8]. They derived the fixed point and limit cycle solutions which we reviewed here, but did not focus on the chaotic regime and they did not discuss the role of network size in the transition out of chaos. Our focus here was on the chaotic regime, both the emergence of coherence for small structured connectivity and the imprint of the non-chaotic regime on the chaotic dynamics for moderate structured connectivity.

A separate study has claimed to observe coherent activity in excitation-inhibition networks of spiking neurons [37]. A study of the dynamics of spiking neurons is beyond the scope of our work, although we would conjecture that coherent activity would arise with orthogonal, rank-one E-I structure in that setting as well.

Previous work has shown how shared inputs from external drive can drive correlated fluctuations in excitation-inhibition networks [6, 25]. In our current work, in the context of rate neurons, we show that such correlated fluctuations can be generated internally by a recurrent network without external drive. In order to avoid either saturation or pure oscillations the coherent activity mode must not drive itself through a feedback loop. In order to achieve this it is necessary that the structured component embed an effectively-feedforward projection between a pair of orthogonal modes. In parallel, Darshan et al [5] have developed a theory for internally generated correlations in excitation-inhibition networks of binary units. The underlying principle is similar: the recurrent connectivity embeds a purely feedforward structure.

We note that the structured component of connectivity in our network is non-normal. The dynamics of non-normal matrices have drawn a fair amount of interest with suggested functional impact on working memory [7, 9] and amplification [17]. Non-normal matrices embed feedforward structure within recurrent connectivity, and the resulting

bioRxiv preprint doi: https://doi.org/10.1101/350801; this version posted October 1, 2018. The copyright holder for this preprint (which was not certified by peer review) is the author/funder, who has granted bioRxiv a license to display the preprint in perpetuity. It is made available under aCC-BY-NC-ND 4.0 International license.

dynamics even in a linear system are not fully determined by the eigenspectrum but depend on the structure of the corresponding eigenvectors[36]. It has been shown that E-I networks are generally non-normal, and that rank one E-I structure amplifies small differences between excitatory and inhibitory rates driving a large common response [17, 11]. This amplification is related to the way in our network, small fluctuations of the residuals are summed along the output mode and drive coherent fluctuations along the input mode in the regime of passive coherence, but these fluctuations are internally driven by the non-linear dynamics whereas the dynamics in those previous studies were linear. As pointed out in [2], a structured component such as in our model is purely feedforward and can be considered an extreme case of non-normality as it has only zero eigenvalues and therefore all the power in its Schur decomposition is in the off-diagonal. The results here depend on this property and cannot be extended to connectivity with only partial feedforward structure.

Rate model dynamics with a rank-one structured component have been studied in depth recently [24, 16]. Since these works focused on time-averaged activity and not fluctuations they did not observe coherent activity in the case of an outer product of a pair of orthogonal vectors as studied here. These works also differed in that the strength of the structured connectivity was scaled as $1/N$. This scaling is similar to our limit of weak structured connectivity, $J_1 \ll 1$, and guarantees that dynamic mean-field theory holds in the limit of large system size, but in that scaling coherent fluctuations will appear only as a finite-size correction.

It has been previously observed [22] and then proven [34] that adding an orthogonal outer-product to a random matrix generates realization-dependent outliers in the eigenspectrum, and furthermore that these outliers are be removed by row balance. It has been previously observed that performing such a subtraction has significant impact on the resulting dynamics [8, 31]. Yet the relationship between the change in eigenspectrum and the dynamics has not been made clear beyond the basic observations regarding the stability of a fixed-point at zero. Here we suggest that the impact of row balance on the chaotic dynamics is not directly related to the eigenspectrum but that this adjustment should be thought of as effectively subtracting the coherent-mode activity from each individual neuron, thus -preventing feedback loops to the coherent mode. We show that row balance enables the emergence of slow residual dynamics with the coherent mode playing the role of dynamic gain, and that it is crucial for the emergence of self-tuned chaos and highly coherent dynamics.

In conclusion we have presented a simple model which generates coherent chaos in which macroscopic fluctuations emerge through the interplay of random connectivity and a structured component that embeds a feedforward connection from an output mode to an orthogonal input mode.

bioRxiv preprint doi: https://doi.org/10.1101/350801; this version posted October 1, 2018. The copyright holder for this preprint (which was not certified by peer review) is the author/funder, who has granted bioRxiv a license to display the preprint in perpetuity. It is made available under aCC-BY-NC-ND 4.0 International license.

Methods

Exact Decomposed Dynamics and Row Balance

We write the full dynamics without row balance:

$$\frac{\mathrm{d}\mathbf{h}}{\mathrm{d}t} = -\mathbf{h} + \mathbf{J}\boldsymbol{\phi} + \frac{J_1}{\sqrt{N}}\boldsymbol{\xi}\boldsymbol{\nu}^T\boldsymbol{\phi} \tag{28}$$

and we define

$$\bar{h} \equiv \frac{1}{N}\boldsymbol{\xi}^T\mathbf{h} \quad \bar{\phi} \equiv \frac{1}{N}\boldsymbol{\xi}^T\boldsymbol{\phi} \tag{29}$$

$$\delta\mathbf{h} \equiv \mathbf{h} - \bar{h}\boldsymbol{\xi} \quad \delta\boldsymbol{\phi} = \boldsymbol{\phi} - \bar{\phi}\boldsymbol{\xi} \tag{30}$$

Applying these definitions to the full dynamics (and noting that $\boldsymbol{\nu}^T\boldsymbol{\phi} = \boldsymbol{\nu}^T\delta\boldsymbol{\phi}$), the exact coherent mode dynamics are

$$\frac{\mathrm{d}\bar{h}}{\mathrm{d}t} = -\bar{h} + \frac{J_1}{\sqrt{N}}\boldsymbol{\nu}^T\delta\boldsymbol{\phi} + \frac{\boldsymbol{\xi}^T}{N}\mathbf{J}\boldsymbol{\phi} \tag{31}$$

and by subtracting these from the full dynamics of $\mathbf{h}$, the decomposed dynamics are:

$$\frac{\mathrm{d}\delta\mathbf{h}}{\mathrm{d}t} = -\delta\mathbf{h} + \mathbf{J}\boldsymbol{\phi} - \frac{\boldsymbol{\xi}\boldsymbol{\xi}^T}{N}\mathbf{J}\boldsymbol{\phi} = -\delta\mathbf{h} + \hat{\mathbf{J}}\boldsymbol{\phi} \tag{32}$$

where $\hat{\mathbf{J}} \equiv \left(\mathbf{I} - \frac{\boldsymbol{\xi}\boldsymbol{\xi}^T}{N}\right)\mathbf{J}$ as introduced in the main text.

We observe that the constraint $\boldsymbol{\xi}^T\delta\mathbf{h} = 0$ must be satisfied automatically by the residual dynamics (Eqn 32), and this can be confirmed by verifying that

$$\frac{\mathrm{d}\left(\boldsymbol{\xi}^T\delta\mathbf{h}\right)}{\mathrm{d}t} = -\left(\boldsymbol{\xi}^T\delta\mathbf{h}\right) \tag{33}$$

In the regime where $J_1 \ll 1$ the ϕ_j are nearly uncorrelated and therefore $\frac{\boldsymbol{\xi}^T}{N}\mathbf{J}\boldsymbol{\phi} \sim O\left(\frac{1}{\sqrt{N}}\right)$ and can be ignored.

In the regime with strong structured connectivity we must consider this term in Eqn 31. To that end we write $\boldsymbol{\phi} = \bar{\phi}\boldsymbol{\xi} + \delta\boldsymbol{\phi}$ and also write the transformation of the input mode via the random matrix as

$$\mathbf{J}\boldsymbol{\xi} = a_{\parallel}\boldsymbol{\xi} + \boldsymbol{\xi}^{\perp} \tag{34}$$

where $a_{\parallel}$ is a realization-dependent scalar and $\boldsymbol{\xi}^{\perp}$ is a realization-dependent vector orthogonal to $\boldsymbol{\xi}$. That yields

bioRxiv preprint doi: https://doi.org/10.1101/350801; this version posted October 1, 2018. The copyright holder for this preprint (which was not certified by peer review) is the author/funder, who has granted bioRxiv a license to display the preprint in perpetuity. It is made available under aCC-BY-NC-ND 4.0 International license.

coherent mode dynamics

$$\frac{\mathrm{d}\bar{h}}{\mathrm{d}t} = -\bar{h} + \frac{J_1}{\sqrt{N}}\boldsymbol{\nu}^T\delta\boldsymbol{\phi} + a_{\parallel}\bar{\phi} + \frac{\boldsymbol{\xi}^T}{N}\mathbf{J}\delta\boldsymbol{\phi} \tag{35}$$

and residual dynamics

$$\frac{\mathrm{d}\delta\mathbf{h}}{\mathrm{d}t} = -\delta\mathbf{h} + \hat{\mathbf{J}}\delta\boldsymbol{\phi} + \bar{\phi}\boldsymbol{\xi}^{\perp} \tag{36}$$

As J_1 increases and the fluctuations in the coherent activity, $\bar{\phi}(t)$, drive feedback in two ways. First of all, $\mathbf{J}$ maps the coherent activity back along the input mode driving direct feedback to the coherent current $\bar{h}$ via the term $a_{\parallel}\bar{\phi}$.

Secondly, $\mathbf{J}$ maps the coherent activity in a realization-dependent direction, $\boldsymbol{\xi}^{\perp}$, orthogonal to the input mode. This drives the residual activity fluctuations $\delta\mathbf{h}$ via the term $\bar{\phi}\boldsymbol{\xi}^{\perp}$, and this biasing of the residual fluctuations may in turn generate feedback to the coherent current through the output mode via $\boldsymbol{\nu}^T\delta\boldsymbol{\phi}$.

Both of these feedback terms are realization dependent, and both of them are canceled via the row balance subtraction

$$\tilde{\mathbf{J}} \equiv \mathbf{J} - \mathbf{J}\frac{\boldsymbol{\xi}\boldsymbol{\xi}^T}{N} \tag{37}$$

which yields exact coherent mode dynamics

$$\frac{\mathrm{d}\bar{h}}{\mathrm{d}t} = -\bar{h} + \frac{J_1}{\sqrt{N}}\boldsymbol{\nu}^T\delta\boldsymbol{\phi} + \frac{\boldsymbol{\xi}^T}{N}\mathbf{J}\delta\boldsymbol{\phi} \tag{38}$$

and residual dynamics

$$\frac{\mathrm{d}\delta\mathbf{h}}{\mathrm{d}t} = -\delta\mathbf{h} + \hat{\mathbf{J}}\delta\boldsymbol{\phi} \tag{39}$$

And in this case the residual dynamics are again uncorrelated so that $\frac{\boldsymbol{\xi}^T}{N}\mathbf{J}\delta\boldsymbol{\phi} \sim O\left(\frac{1}{\sqrt{N}}\right)$ and can again be ignored in the coherent mode dynamics.

Note that $\bar{\phi}$ no longer drives feedback to either the residual or the coherent dynamics. Nevertheless the dynamics are still coupled in both directions as $\delta\boldsymbol{\phi}$ depends on $\bar{h}$.

Perturbative Dynamic Mean-Field Theory in the Limit of Weak Structured Connectivity

We derive the dynamic mean-field equations in the limit of small J_1 using a perturbative approach. We write the mean-field dynamics of the residuals as

$$\frac{\mathrm{d}\delta h_i}{\mathrm{d}t} = -\delta h_i + \eta_i \tag{40}$$

bioRxiv preprint doi: https://doi.org/10.1101/350801; this version posted October 1, 2018. The copyright holder for this preprint (which was not certified by peer review) is the author/funder, who has granted bioRxiv a license to display the preprint in perpetuity. It is made available under aCC-BY-NC-ND 4.0 International license.

and the coherent component as

$$\frac{\mathrm{d}\bar{h}}{\mathrm{d}t} = -\bar{h} + J_1 m \tag{41}$$

where η_i and m are assumed to be uncorrelated, mean-zero Gaussians. For general J_1 the assumption of Gaussianity fails, therefore we assume $J_1 \ll 1$.

The autocorrelation of η_i is given by

$$[\langle \eta_i(t)\, \eta_i(t+\tau)\rangle] = \left[\sum_{j,k} J_{ij} J_{ik} \langle \phi_j(t)\, \phi_k(t+\tau)\rangle\right] \tag{42}$$

where we have introduced [] as the notation for averaging over realizations. We assume that ϕ_j is independent of J_{ij} and so the terms $j \neq k$ have average zero over realizations and we get

$$[\langle \eta_i(t)\, \eta_i(t+\tau)\rangle] = g^2 C(\tau) \tag{43}$$

where

$$C(\tau) \equiv [\langle \phi_j(t)\, \phi_j(t+\tau)\rangle] \tag{44}$$

The autocorrelation of m is given by

$$[\langle m(t)\, m(t+\tau)\rangle] = \frac{J_1^2}{N}\left[\sum_{j,k} \nu_j \nu_k \phi_j(t)\, \phi(t+\tau)\right] \tag{45}$$

And again the $j \neq k$ terms fall in the realization average so that

$$[\langle m(t)\, m(t+\tau)\rangle] = J_1^2 C(\tau) \tag{46}$$

Next we define the autocorrelation of the residuals

$$\Delta_\delta(\tau) \equiv [\langle \delta h_i(t)\, \delta h_i(t+\tau)\rangle] \tag{47}$$

and the autocorrelation of the coherent current

$$\bar{\Delta}(\tau) \equiv \left[\left\langle \bar{h}(t)\, \bar{h}(t+\tau)\right\rangle\right] \tag{48}$$

bioRxiv preprint doi: https://doi.org/10.1101/350801; this version posted October 1, 2018. The copyright holder for this preprint (which was not certified by peer review) is the author/funder, who has granted bioRxiv a license to display the preprint in perpetuity. It is made available under aCC-BY-NC-ND 4.0 International license.

and we can follow previous work [30, 12] and write the dynamic mean-field equations for $\Delta_\delta(\tau)$ as

$$\left(1-\frac{\partial^2}{\partial\tau^2}\right)\Delta_\delta(\tau)=g^2C(\tau) \tag{49}$$

and for $\bar{\Delta}(\tau)$ as

$$\left(1-\frac{\partial^2}{\partial\tau^2}\right)\bar{\Delta}(\tau)=J_1^2C(\tau) \tag{50}$$

Next we note that for $J_1 \ll g$ we assume that $\left|\bar{h}\right| \ll 1$ so we have $\phi_i = \phi\left(\delta h_i + \xi_i\bar{h}\right) \approx \phi(\delta h_i) + \xi_i\phi'(\delta h_i)\bar{h}$. Therefore we have that to leading order

$$C(\tau) \approx \left[\left\langle\phi(\delta h_i(t))\,\phi(\delta h_i(t+\tau))\right\rangle\right] \tag{51}$$

and then following previous results [30, 12] we can write this to leading order as an integral over Gaussians:

$$C(\tau) \approx \int_{-\infty}^{\infty} Dz\left(\int_{-\infty}^{\infty} Dx\,\phi\left(\sqrt{\Delta_\delta(0)-\Delta_\delta(\tau)}x+\sqrt{\Delta_\delta(\tau)}z\right)\right)^2 \tag{52}$$

Note that it is possible to compute the sub-leading correction term as well, but for our purposes this is unnecessary. We suffice it to observe that to leading order, the self-consistency equation for $\Delta_\delta(\tau)$ (Eqn 49) reduces to the identical equation for that of a random network without structured component ($J_1 = 0$)[30], and that $\bar{\Delta}(\tau)$ contributes only to the sub-leading correction. Following [30, 12] then Eqn 49 can be solved yielding $\Delta_\delta(\tau) \approx \Delta_0(\tau)$, where $\Delta_0(\tau)$ is the autocorrelation when $J_1 = 0$.

The dynamic equation for $\bar{\Delta}(\tau)$ is identical to that for $\Delta_\delta(\tau)$ except with J_1 in place of g, so we conclude that the resulting leading order autocorrelation of the coherent mode is

$$\bar{\Delta}(\tau) \approx \frac{J_1^2}{g^2}\Delta_0(\tau) \tag{53}$$

Thus for $J_1 \ll g$ fluctuations in the coherent input are driven passively by the random source which is generated self-consistently by the residual fluctuations, and the resulting autocorrelation of the coherent mode is simply a scaled version of the autocorrelation of the residuals.

It is worth noting that for $J_1 \sim g$ the assumption of Gaussianity is broken due to the cross-correlations between the ϕ_j.

bioRxiv preprint doi: https://doi.org/10.1101/350801; this version posted October 1, 2018. The copyright holder for this preprint (which was not certified by peer review) is the author/funder, who has granted bioRxiv a license to display the preprint in perpetuity. It is made available under aCC-BY-NC-ND 4.0 International license.

Analysis of Fixed Points and Limit Cycles in the Limit of Strong Structured Connectivity

In the limit of large J_1 we assume $\delta h_i \ll 1$, and approximate $\phi_j \approx \phi\left(\xi_j \bar{h}\right) + \phi'\left(\bar{h}\right)\delta h_j$, where we have made use of the symmetry of the transfer function and the binary restriction on ξ_j. Note that this linearization clearly holds without symmetric transfer function for the case of uniform $\xi_j = 1$ as well.

Following the exact decomposition above (Eqns 32 and 31)this yields dynamical equations:

$$\frac{\mathrm{d}\delta\mathbf{h}}{\mathrm{d}t} = -\delta\mathbf{h} + \phi'\left(\bar{h}\right)\hat{\mathbf{J}}\delta\mathbf{h} \tag{54}$$

$$\frac{\mathrm{d}\bar{h}}{\mathrm{d}t} = -\bar{h} + \frac{J_1}{\sqrt{N}}\phi'\left(\bar{h}\right)\boldsymbol{\nu}^T\delta\mathbf{h} + \phi'\left(\bar{h}\right)\frac{\boldsymbol{\xi}^T}{N}\mathbf{J}\delta\mathbf{h} \tag{55}$$

Note that the leading term of the linearization, $\phi\left(\xi_i\bar{h}\right) = \xi_i\phi\left(\bar{h}\right)$ has fallen from all terms, so that in this regime the coupling between residuals and coherent mode has been greatly simplified: The residuals serve as the input while the coherent mode acts as a dynamic gain. This reflects the important role of the orthogonality of $\boldsymbol{\nu}$ and $\boldsymbol{\xi}$ on the one hand, and the row balance subtraction we made to the random connectivity, both of which ensure that the coherent mode does not drive a feedback loop.

In this regime $\bar{h}$ acts as a dynamic gain on the local synaptic currents through $\phi'\left(\bar{h}\right)$. Given $\bar{h}$ the equation for the residual currents is linear and therefore their dynamics can be decomposed in the eigenbasis of the matrix

$$\hat{\mathbf{J}} \equiv \mathbf{P}_\xi\mathbf{J} \tag{56}$$

where $\mathbf{P}_\xi = \mathbf{I} - \frac{\boldsymbol{\xi}\boldsymbol{\xi}^T}{N}$ is the projection matrix onto the the subspace orthogonal to $\boldsymbol{\xi}$. We observe a fine-point not noted in [8]: Had we ignored the constraint $\boldsymbol{\xi}^T\delta\mathbf{h} = 0$ then the residual dynamics would have been determined by $\mathbf{J}$ and its eigenvalues, and these are not the same as those of $\hat{\mathbf{J}}$.

We claim that $\hat{\mathbf{J}} = \mathbf{P}_\xi\mathbf{J}$ and $\tilde{\mathbf{J}} = \mathbf{J}\mathbf{P}_\xi$ have the same eigenvalues. If λ is an eigenvalue $\mathbf{J}$ such that the associated eigenvector $\mathbf{u}$ is orthogonal to $\boldsymbol{\xi}$, then clearly $\mathbf{u}$ is also an eigenvector of both $\hat{\mathbf{J}}$ and $\tilde{\mathbf{J}}$ with the same eigenvalue λ. Otherwise λ is an eigenvalue of both $\hat{\mathbf{J}}$ and $\tilde{\mathbf{J}}$ if and only if $\left(\mathbf{J} - \lambda\mathbf{I}\right)^{-1}\boldsymbol{\xi} = \mathbf{u}$ is orthogonal to $\boldsymbol{\xi}$. In this case it can be readily verified that $\mathbf{u}$ is an eigenvector of $\hat{\mathbf{J}}$, and $\mathbf{J}\mathbf{u} = \lambda\mathbf{u} + \boldsymbol{\xi}$ is an eigenvector of $\tilde{\mathbf{J}}$. Thus we note also that the eigenvectors of $\hat{\mathbf{J}}$are orthogonal to $\boldsymbol{\xi}$ (except potentially for one eigenvector with zero eigenvalue).

bioRxiv preprint doi: https://doi.org/10.1101/350801; this version posted October 1, 2018. The copyright holder for this preprint (which was not certified by peer review) is the author/funder, who has granted bioRxiv a license to display the preprint in perpetuity. It is made available under aCC-BY-NC-ND 4.0 International license.

We write the eigenvectors as $\mathbf{u}^{(i)}$ with $\hat{\mathbf{J}} \cdot \mathbf{u}^{(i)} = \lambda_i \mathbf{u}^{(i)}$. Writing the vector of residual current as $\delta\mathbf{h} = \sum_i c_i \mathbf{u}^{(i)}$ yields dynamics

$$\frac{\mathrm{d}c_i}{\mathrm{d}t} = \left(-1 + \phi'\left(\bar{h}\right)\lambda_i\right) c_i \tag{57}$$

The only (marginally) stable, non-zero fixed point is achieved with $c_1 \neq 0$ and $c_i = 0$ for all $i > 1$. And the fixed-point equation is

$$c_1^* \left(1 - \phi'\left(\bar{h}\right)\lambda_1\right) = 0 \tag{58}$$

This fixed point only exists if λ_1 is real, and yields a fixed-point requirement for $\bar{h}^*$:

$$\bar{h}^* = \phi'^{-1}\left(\frac{1}{\lambda_1}\right) \approx \phi'^{-1}\left(\frac{1}{g}\right) \tag{59}$$

In order to close the loop we turn to the fixed point equation for the coherent dynamics. Ignoring the term $\phi'\left(\bar{h}\right)\frac{\boldsymbol{\xi}^T}{N}\mathbf{J}\delta\mathbf{h}$, which yields an $O\left(\frac{1}{\sqrt{N}}\right)$ correction we find:

$$\bar{h}^* = \frac{J_1}{\sqrt{N}}\phi'\left(\bar{h}\right)\boldsymbol{\nu}^T\delta\mathbf{h}^* \tag{60}$$

which in turn, using $\delta\mathbf{h}^* = c_1\mathbf{u}^{(1)}$, yields a solution to leading order for c_1: $c_1^* = \frac{\sqrt{N}\bar{h}^*\lambda_1}{J_1\boldsymbol{\nu}^T\mathbf{u}^{(1)}}$, as reported in [8].

If λ_1 is complex there is no fixed point but rather a limit-cycle solution to the dynamics of the complex-valued c_1 exists with $\delta\mathbf{h}\left(t\right) = \mathrm{Re}\left[c_1\left(t\right)\mathbf{u}^{(1)}\right]$, and $c_i = 0$ for all other eigenmodes. Assuming $\bar{h}\left(t\right)$ is periodic with period T, we can separate variables and integrate Eqn 57 in order to find $c_1\left(t\right)$ is given by

$$c_1\left(t\right) = c_1\left(0\right)\exp\left(-t + \lambda_1\Phi\left(t\right)\right) \tag{61}$$

for $t \leq T$, where $\Phi\left(t\right) = \int_0^t \mathrm{d}s\,\phi'\left(\bar{h}\left(s\right)\right)$. Writing $c_1\left(0\right) = \left|c_1^0\right|\exp\left(i\theta_0\right)$ and using $\mathrm{Re}\lambda_1 \approx g$, this gives

$$c_1\left(t\right) = \left|c_1^0\right|\exp\left(-t + g\Phi\left(t\right)\right)\exp\left(i\left(\theta_0 + \mathrm{Im}\lambda_1\Phi\left(t\right)\right)\right) \tag{62}$$

A limit cycle in phase with $\bar{h}\left(t\right)$ means $c_1\left(T\right) = c_1\left(0\right)$ and this requires that both $g\Phi\left(T\right) = T$ and also $\mathrm{Im}\left[\lambda_1\right]\Phi\left(T\right) = 2\pi$. From the first requirement we find that the average value of ϕ' over a period must be the critical value:

$$\left\langle\phi'\left(\bar{h}\right)\right\rangle = \frac{\Phi\left(T\right)}{T} = \frac{1}{g}. \tag{63}$$

bioRxiv preprint doi: https://doi.org/10.1101/350801; this version posted October 1, 2018. The copyright holder for this preprint (which was not certified by peer review) is the author/funder, who has granted bioRxiv a license to display the preprint in perpetuity. It is made available under aCC-BY-NC-ND 4.0 International license.

And combining the second requirement yields an expression for the period (Eqn 18, as reported in [8] as well):

$$T = 2\pi \frac{\mathrm{Re}\lambda_1}{\mathrm{Im}\lambda_1} \tag{64}$$

We can further write a self-consistency expression for $\bar{h}(t)$ by taking $c_1(t)$ as given by Eqn 62 and integrate over the coherent mode dynamics:

$$\frac{\mathrm{d}\bar{h}}{\mathrm{d}t} = -\bar{h} + \mathrm{Re}\left[\frac{J_1}{\sqrt{N}}\boldsymbol{\nu}^T\mathbf{u}^{(1)}c_1(0)\,\phi'\left(\bar{h}(t)\right)\exp\left(-t+\lambda_1\Phi(t)\right)\right] \tag{65}$$

which yields

$$\bar{h}(t) = \bar{h}(0)\exp(-t) + \mathrm{Re}\left[\frac{J_1}{\sqrt{N}}\frac{\boldsymbol{\nu}^T\mathbf{u}^{(1)}}{\lambda_1}c_1(0)\exp\left(-t+\lambda_1\Phi(t)\right)\right] \tag{66}$$

Without loss of generality we assume that $\bar{h}(0) = \bar{h}^c = \phi'^{-1}\left(\frac{1}{g}\right)$, then

$$\bar{h}^c \approx c_1^0\frac{J_1\left|\boldsymbol{\nu}^T\mathbf{u}^{(1)}\right|}{\sqrt{N}g}\cos\left(\theta_0 + \mathrm{Im}\left(\boldsymbol{\nu}^T\mathbf{u}^{(1)}\right)\right) \tag{67}$$

This is analogous to the fixed point equation for $\bar{h}^*$ and c_1^*. In both cases the requirement that $\delta h_i = c_1 u_i^{(1)} \ll 1$ requires that c_1 be maximally $O(1)$ and motivates our conjectures about the realization-dependence and system-size scaling of the transition out of chaos. In particular, we expect and confirm numerically that the critical value of J_1 for transition to either fixed point or limit cycle is inversely proportional to $\left|\boldsymbol{\nu}^T\mathbf{u}^{(1)}\right|$ and grows with network size (see main text and Fig 7).

In the case of complex leading eigenvalue, simulations confirm that a projection of the full synaptic current dynamics into the coherent mode and the leading eigenvector plane (consisting of real and imaginary parts of $\mathbf{u}^{(1)}$) accounts for well over 0.99 of the total variance. Even restricting ourselves to the variance of the residuals, δh_i, we find that 0.98 of the variance is restricted to the leading eigenvector plane (Fig S3).

For $N = 4000$ we simulate 219 realizations of random connectivity with complex leading eigenvalue and find that for sufficiently large J_1 all but one of these realizations yield highly oscillatory dynamics with period predicted nearly perfectly by theory (Fig S3).

We note that in the limit of large N we expect that the typical size of the imaginary component of the leading eigenvalue, λ_1, shrinks such that the typical period grows. These longer period oscillations are characterized by square-wave-like shape in which the dynamics of the coherent component slows around the critical value $\bar{h}^c = \phi^{-1}\left(\frac{1}{\mathrm{Re}\lambda_1}\right)$, which is identical to the fixed-point value of $\bar{h}$ when λ_1 is real. (Fig S3)

bioRxiv preprint doi: https://doi.org/10.1101/350801; this version posted October 1, 2018. The copyright holder for this preprint (which was not certified by peer review) is the author/funder, who has granted bioRxiv a license to display the preprint in perpetuity. It is made available under aCC-BY-NC-ND 4.0 International license.

The fraction of realizations with real leading eigenvalue in the large N limit has not been calculated analytically to our knowledge. We find numerically that this fraction appears to saturate roughly around $\frac{3}{10}$ for $N \gtrsim 8000$.

Lyapunov Exponent, Limit Cycles, and Fixed Points

In order to calculate the largest Lyapunov exponent, we begin with a point $\mathbf{h}_0$ along the trajectory of the dynamics and we solve concurrently for the dynamics of the trajectory, $\mathbf{h}(t)$ with $\mathbf{h}(0) = \mathbf{h}_0$, and for a randomly chosen perturbation, $\boldsymbol{\eta}(t)$. The trajectory $\mathbf{h}(t)$ yields the time-dependent Jacobian matrix for each point along the trajectory:

$$\mathcal{J}_{ij}(t) = -1 + J_{ij}\phi'(h_j(t)) \tag{68}$$

We choose a random unit-norm vector $\boldsymbol{\eta}(0) = \boldsymbol{\eta}_0$ and iterate the linearized dynamics of the perturbation:

$$\frac{\mathrm{d}\boldsymbol{\eta}}{\mathrm{d}t} = \boldsymbol{\mathcal{J}}\boldsymbol{\eta} \tag{69}$$

The largest Lyapunov exponent is given by

$$\lim_{t\to\infty} \frac{1}{t} \log \|\boldsymbol{\eta}(t)\| \tag{70}$$

In practice we iterate 69 until $t = 5000$, that is, 5000 times the intrinsic time-scale of the dynamics, and we renormalize $\boldsymbol{\eta}(t)$ at intervals of $t = 100n$ for $n = \{1, 2, ..., 50\}$.

We classify fixed points numerically by a threshold on the fluctuations of the coherent input: $\mathrm{std}\left(\bar{h}(t)\right) \leq 5\mathrm{x}10^{-4}$.

We classify limit cycles by a threshold on the second peak of the normalized coherent autocorrelation: $q_{peak} \geq 0.9$.

We confirm that all of the trials with negative Lyapunov exponent were categorized as either fixed points or limit cycles. A small fraction of trials classified as limit cycles had positive Lyapunov exponents but with the largest one 0.0043.

Acknowledgements

We thank Rainer Engelken for advice on numerically calculating Lyapunov exponents, and Yu Hu for very helpful comments on the manuscript. We thank the anonymous reviewers for thorough questions that helped clarify the manuscript.

bioRxiv preprint doi: https://doi.org/10.1101/350801; this version posted October 1, 2018. The copyright holder for this preprint (which was not certified by peer review) is the author/funder, who has granted bioRxiv a license to display the preprint in perpetuity. It is made available under aCC-BY-NC-ND 4.0 International license.

References

[1] Peter Achermann, Thomas Rusterholz, Roland Dürr, Thomas König, and Leila Tarokh. Global field synchronization reveals rapid eye movement sleep as most synchronized brain state in the human EEG. *Royal Society Open Science*, 3(10):160201, 2016.

[2] Yashar Ahmadian, Francesco Fumarola, and Kenneth D. Miller. Properties of networks with partially structured and partially random connectivity. *Physical Review E - Statistical, Nonlinear, and Soft Matter Physics*, 91(1):1–36, 2015.

[3] Anne K. Churchland, R. Kiani, R. Chaudhuri, Xiao Jing Wang, Alexandre Pouget, and M. N. Shadlen. Variance as a Signature of Neural Computations during Decision Making. *Neuron*, 69(4):818–831, 2011.

[4] Marlene R. Cohen and John H.R. Maunsell. Attention improves performance primarily by reducing interneuronal correlations. *Nature Neuroscience*, 12(12):1594–1600, 2009.

[5] Ran Darshan, Carl van Vreeswijk, and David Hansel. Strength of correlations in strongly recurrent neural networks. *Physical Review X*, 2018.

[6] Ran Darshan, William E. Wood, Susan Peters, Arthur Leblois, and David Hansel. A canonical neural mechanism for behavioral variability. *Nature Communications*, 8(May):15415, 2017.

[7] Surya Ganguli, Dongsung Huh, and Haim Sompolinsky. Memory traces in dynamical systems. *Proceedings of the ...*, 105(48):18970–18975, 2008.

[8] Luis Carlos García Del Molino, Khashayar Pakdaman, Jonathan Touboul, and Gilles Wainrib. Synchronization in random balanced networks. *Physical Review E - Statistical, Nonlinear, and Soft Matter Physics*, 88(4):1–5, 2013.

[9] Mark S Goldman. Memory without Feedback in a Neural Network. *Neuron*, 61(4):621–634, 2009.

[10] Takashi Hayakawa and Tomoki Fukai. Spontaneous and stimulus-induced coherent states of dynamically balanced neuronal networks. *arXiv*, (1):1–36, 2018.

[11] Guillaume Hennequin, Tim P. Vogels, and Wulfram Gerstner. Non-normal amplification in random balanced neuronal networks. *Physical Review E - Statistical, Nonlinear, and Soft Matter Physics*, 86(1):1–12, 2012.

[12] Jonathan Kadmon and Haim Sompolinsky. Transition to chaos in random neuronal networks. *Physical Review X*, 5(4):1–28, 2015.

[13] Itamar D Landau, Robert Egger, Vincent J Dercksen, Marcel Oberlaender, and Haim Sompolinsky. The Impact of Structural Heterogeneity on Excitation-Inhibition Balance in Cortical Networks. *Neuron*, 92:http://dx.doi.org/10.1016/j.neuron.2016.10.027, 2016.

bioRxiv preprint doi: https://doi.org/10.1101/350801; this version posted October 1, 2018. The copyright holder for this preprint (which was not certified by peer review) is the author/funder, who has granted bioRxiv a license to display the preprint in perpetuity. It is made available under aCC-BY-NC-ND 4.0 International license.

[14] Thomas T. Liu, Alican Nalci, and Maryam Falahpour. The global signal in fMRI: Nuisance or Information? *NeuroImage*, 150(February):213–229, 2017.

[15] Yotam Luz and Maoz Shamir. Balancing feed-forward excitation and inhibition via Hebbian inhibitory synaptic plasticity. *PLoS computational biology*, 8(1):e1002334, jan 2012.

[16] Francesca Mastrogiuseppe and Srdjan Ostojic. Linking connectivity, dynamics and computations in recurrent neural networks. *Neuron*, 99(3):609–623.e29, 2018.

[17] Brendan K Murphy and Kenneth D Miller. Balanced Amplification: A New Mechanism of Selective Amplification of Neural Activity Patterns. *Neuron*, 61(4):635–648, 2009.

[18] Kevin Murphy and Michael D. Fox. Towards a consensus regarding global signal regression for resting state functional connectivity MRI. *NeuroImage*, 154:169–173, 2017.

[19] P L Nunez, R B Silberstein, M R Carpentar, R Srinivisan andR.S. Wijesinghe, D M Tucker, P J Cadusch, and X Wu. EEG coherency II: Experimental comparison of multiple measures. *Electroenceaphlogr Clin Neurophysiol*, 110:469, 1999.

[20] M. Okun, P. Yger, S. L. Marguet, F. Gerard-Mercier, A. Benucci, S. Katzner, L. Busse, M. Carandini, and K. D. Harris. Population Rate Dynamics and Multineuron Firing Patterns in Sensory Cortex. *Journal of Neuroscience*, 32(48):17108–17119, 2012.

[21] Michael Okun, Nicholas a. Steinmetz, Lee Cossell, M. Florencia Iacaruso, Ho Ko, Péter Barthó, Tirin Moore, Sonja B. Hofer, Thomas D Mrsic-Flogel, Matteo Carandini, and Kenneth D Harris. Diverse coupling of neurons to populations in sensory cortex. *Nature*, 2015.

[22] Kanaka Rajan and L F Abbott. Eigenvalue Spectra of Random Matrices for Neural Networks. *Physical Review Letters*, 97(18):188104, nov 2006.

[23] Alfonso Renart, Jaime De Rocha, Peter Bartho, Liad Hollender, Néstor Parga, Alex Reyes, and Kenneth D Harris. The Asynchronous State in Cortical Circuits. *Science (New York, N.Y.)*, 327(January):587–590, 2010.

[24] Alexander Rivkind and Omri Barak. Local Dynamics in Trained Recurrent Neural Networks. *Physical Review Letters*, 118(25):1–5, 2017.

[25] Robert Rosenbaum, Matthew A Smith, Adam Kohn, Jonathan E Rubin, and Brent Doiron. The spatial structure of correlated neuronal variability. *Nature Neuroscience*, 20(October):1–35, 2016.

[26] M. L. Scholvinck, A. Maier, F. Q. Ye, J. H. Duyn, and D. A. Leopold. Neural basis of global resting-state fMRI activity. *Proceedings of the National Academy of Sciences*, 107(22):10238–10243, 2010.

bioRxiv preprint doi: https://doi.org/10.1101/350801; this version posted October 1, 2018. The copyright holder for this preprint (which was not certified by peer review) is the author/funder, who has granted bioRxiv a license to display the preprint in perpetuity. It is made available under aCC-BY-NC-ND 4.0 International license.

[27] Matthew a Smith and Adam Kohn. Spatial and temporal scales of neuronal correlation in primary visual cortex. *The Journal of neuroscience : the official journal of the Society for Neuroscience*, 28(48):12591–603, nov 2008.

[28] W R Softky and C Koch. The highly irregular firing of cortical cells is inconsistent with temporal integration of random EPSPs. *The Journal of neuroscience : the official journal of the Society for Neuroscience*, 13(1):334–50, jan 1993.

[29] H. Sompolinsky and I. Kanter. Temporal association in asymmetric neural networks. *Physical Review Letters*, 57(22):2861–2864, 1986.

[30] Haim Sompolinsky, A. Crisanti, and H. J. Sommers. Chaos in random neural networks. *Physical Review ...*, 61(3):259–262, 1988.

[31] Merav Stern and L F Abbott. Dynamics of rate-model networks with seperate excitatory and inhibitory populations. *The annual meeting of the Society for Neuroscience*, 2016.

[32] David Sussillo and Omri Barak. Opening the black box: low-dimensional dynamics in high-dimensional recurrent neural networks. *Neural computation*, 25(3):626–49, mar 2013.

[33] David W Tank and J J Hopfield. Neural computation by concentrating information in time. *Proceedings of the National Academy of Sciences*, 84(April):1896–1900, 1987.

[34] Terence Tao. Outliers in the spectrum of iid matrices with bounded rank perturbations. *Probability Theory and Related Fields*, 155(1-2):231–263, 2013.

[35] B Tirozzi and M Tsodyks. Chaos in highly diluted neural networks. *EPL (Europhysics Letters)*, 14(8):727–732, 1991.

[36] Lloyd N. Trefethen and Mark Embree. *Spectra and pseudospectra: the behavior of nonnormal matrices and operators*. Princeton University Press, 2005.

[37] Ekkehard Ullner, Antonio Politi, and Alessandro Torcini. Collective irregular dynamics in balanced networks of leaky integrate-and-fire neurons. 081106, 2018.

[38] Carl van Vreeswijk and Haim Sompolinsky. Chaotic balanced state in a model of cortical circuits. *Neural computation*, 10(6):1321–71, aug 1998.

[39] Tim P Vogels, H Sprekeler, F Zenke, C Clopath, and W Gerstner. Inhibitory plasticity balances excitation and inhibition in sensory pathways and memory networks. *Science (New York, N.Y.)*, 334(6062):1569–73, dec 2011.

bioRxiv preprint doi: https://doi.org/10.1101/350801; this version posted October 1, 2018. The copyright holder for this preprint (which was not certified by peer review) is the author/funder, who has granted bioRxiv a license to display the preprint in perpetuity. It is made available under aCC-BY-NC-ND 4.0 International license.

[40] Maxim Volgushev, Sylvain Chauvette, and Igor Timofeev. Long-range correlation of the membrane potential in neocortical neurons during slow oscillation. *Progress in Brain Research*, 193:181–199, 2011.

bioRxiv preprint doi: https://doi.org/10.1101/350801; this version posted October 1, 2018. The copyright holder for this preprint (which was not certified by peer review) is the author/funder, who has granted bioRxiv a license to display the preprint in perpetuity. It is made available under aCC-BY-NC-ND 4.0 International license.

Supporting Information Legends

Figure S1 (see Fig 4). Self-Tuned Coherent Dynamics With Non-Symmetric Transfer Function. (A) We use a non-symmetric transfer function $\phi(h) = (1 + \exp -\beta h)^{-p}$ with $\beta = 4$ and $p = \frac{1}{2}$. **(B)** Activity trace of coherent activity $\bar{\phi}(t)$ in black and 10 randomly chosen neurons $\phi_i(t)$ displays coherent switching between slow states. **(C)** Histogram of values of coherent current, $\bar{h}$, displays bimodality with peaks near the critical values predicted by theory where $\phi'\left(\bar{h}\right) = \frac{1}{g}$. Simulations for $N = 2000$ and $g = 2$ with row balance.

Figure S2 (see Fig 5). Real Leading Eigenvalues Yield Fixed Points. (A) Sample chaotic dynamics for $J_1 = 0.1$. **(B)** Sample dynamics of same connectivity realization as in (A) but with $J_1 = 1$. **(C)** Scatterplot of all h_i^* at fixed point, plotted against individual components of the leading eigenvector, u_i^1. Red dot is value of coherent mode at FP. Black dashed line is FP value predicted from theory. **(D)** Value of coherent mode at FP, $\bar{h}^*$, as a function of the standard deviation of the random connectivity, g. Black line is prediction from theory: $\bar{h}^c = \text{sech}^{-1}\left(\frac{1}{\sqrt{g}}\right)$. **(E)** Phase diagram for a single realization with real leading eigenvalue. Colormap shows the absolute value of the mean coherent current over a single trial, $\left|\left\langle \bar{h} \right\rangle\right|$ which is close to zero when the network is chaotic and non-zero when at a fixed point. The bar below shows the fixed point value predicted by theory, $\bar{h}^c$, which is independent of J_1. **(F)** Stability eigenvalue at fixed point, i.e. leading eigenvalue of the Jacobian, $-1 + \tilde{J}_{ij}\phi'\left(h_j^*\right)$, as a function of J_1 for a specific realization of the random connectivity. The fixed point exhibits marginal stability independent of J_1. Networks in all panels have row balance. $N = 4000$.

Figure S3 (see Fig 6). Complex Leading Eigenvalues Yield Limit Cycles. (A) Top: Sample chaotic dynamics for $J_1 = 0.25$. Bottom: Autocorrelation of coherent mode shows oscillatory ringing. **(B)** Same connectivity realization as (A) but with $J_1 = 2$. Dashed pink line in top panel is prediction from solving the three-dimensional dynamics. Autocorrelation shows near-perfect oscillations. **(C)** Projection of the full dynamics of (B) onto coherent mode and the real and imaginary parts of the leading eigenvector. These three dimensions account for more than 0.99 of the total variance of the dynamics. Gray projection onto the leading eigenvector plane accounts for 0.98 of the variance of the residual currents. **(D)** Scatterplot of period of oscillations plotted against the phase of the leading eigenvalue, $\frac{\text{Im}\lambda_1}{\text{Re}\lambda_1}$, of $\tilde{\mathbf{J}}$, for 219 different realizations of the random connectivity. Black line shows prediction from theory, $T = 2\pi\frac{\text{Re}\lambda_1}{\text{Im}\lambda_1}$. **(E)** Phase diagram for a single connectivity realization with complex leading eigenvalue. Colormap shows the second peak of the normalized autocorrelation of the coherent mode. Networks in all panels have row balance. $N = 4000$

Figure S4 (see Fig 3). Near Perfect Coherence as Strength of Structured Connectivity is Increased. (A) Plot of coherence, χ, vs strength of structured connectivity, J_1, for networks of size $N = 16000$ with row balance. Dots display average over realizations, bars display standard deviation. Only chaotic realizations included

bioRxiv preprint doi: https://doi.org/10.1101/350801; this version posted October 1, 2018. The copyright holder for this preprint (which was not certified by peer review) is the author/funder, who has granted bioRxiv a license to display the preprint in perpetuity. It is made available under aCC-BY-NC-ND 4.0 International license.

(those not found to be at a fixed point or a limit cycle - see methods). More than 20 realizations per value of J_1. For $J_1 = 100$, 22 out of 30 realizations were chaotic and the average coherence among these realizations was 0.963.